

**Narrow-Angle Astrometry with the Space Interferometry Mission:
The Search for Extra-solar Planets.
I. Detection and Characterization of Single Planets**

A. Sozzetti^{1,2,4}

alex@phyast.pitt.edu

S. Casertano³ and R. A. Brown³

stefano@stsci.edu; rbrown@stsci.edu

and

M. G. Lattanzi⁴

lattanzi@to.astro.it

ABSTRACT

A decade after the publication of the Hipparcos Catalogue, the Space Interferometry Mission (SIM) will be capable of making selected high-precision astrometric measurements about three orders of magnitude more accurate than the Hipparcos survey.

We present results from a detailed set of end-to-end numerical simulations of SIM narrow-angle astrometric measurements and data analysis to illustrate the enormous potential that SIM has for the discovery and characterization of planets outside the Solar System. Utilizing a template observing scenario, we quantify SIM sensitivity to single planets orbiting single normal nearby stars as function of measurement errors and properties of the planet: SIM will detect over 95% of the planets with periods between a few days and the 5-year nominal mission lifetime that produce astrometric signatures ~ 2.2 times larger than the single-measurement accuracy. We provide accuracy estimates of full-orbit reconstruction and planet mass determination: at twice the discovery limit, orbital elements will be determined with a typical accuracy of 20-30%; the astrometric signature must be ~ 10 and ~ 15 times the minimum signal

¹University of Pittsburgh, Dept. of Physics & Astronomy, Pittsburgh, PA 15260, USA

²Smithsonian Astrophysical Observatory, Harvard-Smithsonian Center for Astrophysics, 60 Garden Street, Cambridge, MA 02138

³Space Telescope Science Institute, Baltimore, MD 21218, USA

⁴Osservatorio Astronomico di Torino, 10025 Pino Torinese, Italy

required for detection to derive mass and inclination angle estimates accurate to 10%. We quantify the impact of different observing strategies on the boundaries for secure detection and accurate orbit estimation: the results scale with the square root of both the number of observations and the number of reference stars. We investigate SIM discovery space, to gauge the instrument ability in detecting very low-mass planets: around the nearest stars, SIM will find planets as small as Earth, if they are present. Some of these might be orbiting inside the parent star’s Habitable Zone.

Extra-solar planets figure prominently among SIM scientific goals: our results reaffirm the importance of high-precision astrometric measurements as a unique complement to spectroscopic surveys based on radial velocity. For example, establishing the existence of rocky, perhaps habitable planets would constitute both a fundamental test of theoretical models, and progress towards the understanding of formation and evolution processes of planetary systems. Such discoveries would also provide the Terrestrial Planet Finder (TPF) with prime targets to investigate with direct spectroscopy in terms of the potential for life.

Subject headings: astrometry – planetary systems – instrumentation: interferometers – methods: data analysis – methods: numerical

1. Introduction

Six years ago, research in planetary science was essentially synonymous with studies of our Solar System alone. Only four years later, thanks to extensive precision radial velocity surveys of the solar neighborhood, Butler et al. (2000) could list 50 nearby Main-Sequence stars orbited by at least one planet candidate with projected masses⁵ below the so-called deuterium burning threshold ($M \sin i < 13M_J$, where M_J is the mass of Jupiter), as discussed by Oppenheimer et al. (2000). The number of planets continues to grow; as of July 2002, 26 more candidate planets have been identified, bringing the number of stars harboring planetary-mass companions to 88. Recently, one of these candidate extra-solar planets was confirmed to be a Jupiter-mass object in a few-days period orbit (a *Hot Jupiter*) via transit observations of the star HD 209458 (Henry et al. 2000; Charbonneau et al. 2000), and the presence of sodium in its atmosphere detected (Charbonneau et al. 2002). Furthermore, radial velocity measurements have also proven the existence of candidate planetary *systems* (Butler et al. 1999; Marcy et al. 2001a; Udry et al. 2000; Fischer et al. 2002), and of systems composed of a planet and a brown dwarf candidate (Udry et al. 2000; Marcy et al. 2001b; Els et al. 2001). Except for the case of HD 209458, all low-mass companions to solar-type stars having $M \sin i < 13M_J$ have been classified by some as extra-solar planets solely on the basis of their small projected

⁵Radial velocity techniques cannot determine the viewing geometry of the orbit, and consequently only lower limits to the companion mass can be inferred

masses, and thus, under the reasonable assumption of orbital planes randomly oriented in space, small true masses. In fact, the true nature of such objects is still matter of ongoing debates among the scientific community. For example, the unexpected orbital configurations of the majority of the planet candidates, such as companions having $M \sin i \geq M_J$ and orbital periods of a few days (Mayor & Queloz 1995; Butler et al. 1997) or large eccentric orbits (Mazeh et al. 1996; Cochran et al. 1997) have raised crucial questions about their origin. In response to these challenging discoveries, new theoretical models have been proposed, which invoke diverse mechanisms like orbital migration (Murray et al. 1998; Trilling et al. 1998; Del Popolo & Ekşi 2002) or *in situ* formation (Ward 1997; Wuchterl 1997; Bodenheimer et al. 2000). Statistical analyses have also been carried out (Heacox 1999; Stepinski & Black 2000; Mayor & Udry 2000; Stepinski & Black 2001; Mazeh & Zucker 2001), which, highlighting the striking similarity between the distributions of eccentricities and periods of the two populations, suggest alternative scenarios implying common formation processes for planet and brown dwarf candidates, and for stellar binaries. On the other hand, recent attempts to determine the actual mass distribution of low-mass companions to nearby stars (Mazeh & Zucker 2001; Jorissen et al. 2001; Zucker & Mazeh 2001b; Halbwachs et al. 2001) have confirmed the indications obtained by early studies (Basri & Marcy 1997; Mayor et al. 1998a; Mayor et al. 1998b; Marcy & Butler 1998) which pointed out remarkable differences in the mass distribution of planet candidates and low-mass stellar secondaries. In particular, the two populations appear to be separated by a gap in mass of roughly an order of magnitude in the range 10-100 M_J . This is the so-called “brown-dwarf desert” (see for example the early works of Campbell et al. (1988), Marcy & Benitz (1989), Marcy & Butler (1994), and more recently Halbwachs et al. (2000)), commonly thought of as supporting the idea that the two populations are actually distinct, and therefore suggesting that planet candidates are indeed planets. On the basis of joint analyses of Hipparcos Intermediate Astrometric Data and ground-based astrometric observations, Gatewood et al. (2001) and Han et al. (2001) cast doubts on the actual planetary nature of the low-mass objects detected by radial velocity surveys, disputing the hypothesis of randomness of the orbital planes. Recently, Pourbaix (2001), Pourbaix & Arenou (2001), and Zucker & Mazeh (2001a) have questioned the statistical significance and robustness of their method and results, arguing that the present milli-arcsecond precision of the most accurate astrometric measurements today available is insufficient to derive sensible conclusions on the exact nature of these objects. Furthermore, the Main-Sequence stars harboring the planet candidates have been shown to have higher metallicity than the average of field stars with the same mass in the solar neighborhood (Laughlin 2000; Gonzalez et al. 2001; Santos et al. 2001), and these findings may support the evidence for significant correlation between high stellar metallicity and the presence of orbiting giant planets, under the assumption that core accretion is the primary planet formation mechanism. However, if disk instability is the preferred mechanism for forming extrasolar giant planets, then the metallicity dependence may turn out to be an artifact due to observational selection effects or stellar pollution by ingestion of planetary material, and even low-metallicity stars should harbor giant planets (Boss 2002). As it can be easily understood, such a plethora of diverse interpretations clearly indicates how our present understanding of the origin of planetary

systems is *de facto* still limited, and significant contributions in terms of data obtained via means other than Doppler shift measurements are essential in order to be able to discriminate between biased theoretical and observational models.

Radial velocity surveys, accurate to 3-5 m/s (Butler et al. 1996), have been so far a unique tool for planet discovery. However, we anticipate that high-precision astrometry, both from ground (Mariotti et al. 1998; Booth et al. 1999; Colavita et al. 1999) and in space (Danner & Unwin 1999; Röser 1999; Gilmore et al. 2000), will be among the preferred means for helping fill regions of the parameter space Doppler techniques cannot reach. Astrometry has a significant advantage over the radial velocity technique because it measures two rather than one projection of an orbit and thus describes the full three-dimensional geometry. Astrometry, removing the degeneracy on the inclination angle, provides unambiguous mass estimates and directly determines coplanarity for systems of planets. Astrometric techniques can be used to search for planets around young and bright stars (earlier than F), and late M dwarfs. These objects cannot be searched by radial velocity, either because of their spectral properties (absence of relevant spectral lines) or because of intrinsic instability of the stellar atmospheres (active chromospheres, spots, significant rotation). Furthermore, astrometric sensitivity increases for planets with longer periods, thus complementing radial velocity searches, which favor short-period planets. Finally, radial velocity detection limits are currently of about a Saturn mass within 1 AU. As we will see, astrometry with SIM’s exquisite sensitivity pushes detection two orders of magnitude lower, down to Earth masses.

SIM (Space Interferometry Mission) is under development as NASA’s first space-based optical interferometer devoted to micro-arcsecond (μas) astrometry (Danner & Unwin 1999). It represents a First Generation Mission within NASA’s *Origins* Program (<http://origins.jpl.nasa.gov/>), which has the long-term goal of direct imaging of Earth-like planets around nearby solar-type stars. The instrument is scheduled for launch by mid-2009, with a nominal mission lifetime of 5 years. SIM will perform pointed observations, unlike astrometric missions such as Hipparcos (<http://astro.estec.esa.nl/Hipparcos/>), DIVA (Röser 1999), or the recently approved ESA Cornerstone Mission GAIA (Perryman et al. 2001), which are designed to survey the sky using a well-defined scanning law, in order to build global astrometric catalogues. On one hand, this will limit the total mission throughput. A few tens of thousands objects will be observed, compared to the 120 000 stars surveyed by Hipparcos or to the $10^7 - 10^9$ objects which are expected to be charted by DIVA and GAIA, respectively. On the other hand, SIM’s pointed observations can achieve unprecedented astrometric accuracy that will bring new light in the exploration of our galactic neighborhood.

Detection and measurement of planets will be carried out primarily with SIM operated in narrow-angle astrometric mode. The instrument is expected to achieve a narrow-angle *single measurement* accuracy of $\sim 1 \mu\text{as}$ in 1 hr integration time on bright targets ($V \leq 11$), which corresponds to the amplitude of the gravitational perturbation induced on a solar-mass star by an Earth-mass planet on a 1 AU orbit, as seen from 3 pc. SIM local astrometry is therefore uniquely suited for detection and measurement of planets with masses as small as a few Earth masses in

the vicinity of the Solar System.

This is the first of two papers which will connect and relate the basic SIM capabilities to the properties of extra-solar planetary system. We have built a detailed software suite to *a)* simulate sample narrow-angle SIM observing campaigns of stars with planets, and *b)* analyze the simulated datasets resulting from such observations. The purpose of this first paper is to show how these tools can be used to evaluate the detectability of single planets around single stars and their measurability in terms of mass and orbital characteristics, as a function of both SIM mission parameters and properties of the planet. In the second paper we will address the issues of the detectability and measurability of systems of planets with SIM, as well as extensive analyses of the instrument capability to determine the coplanarity (or non coplanarity) for a variety of orbital arrangements in multiple-planet systems.

The first paper is organized as follows. In the second Section we briefly describe SIM narrow-angle astrometric mode. In the third Section we present a description of the software for the simulation of SIM narrow-angle observations. Details on detection and orbit determination methods are given in the fourth Section. The most significant results obtained so far are presented in the fifth Section, followed by summary and conclusions.

2. SIM Narrow-Angle Astrometric Model

In its current design, the SIM instrument consists of three Michelson interferometers (each composed of two starlight collectors, a beam combiner, and a delay line) with nearly parallel baselines, simultaneously operated at optical wavelengths (0.4–0.9 μm). Eight starlight collectors (siderostats) are distributed along the spacecraft structure (two provide redundancy), so that at any time three interferometers with three different baselines can be selected. An external metrology truss monitors the relative positions of the three baselines. While one interferometer, the “science” interferometer, measures angular positions of the celestial objects in the observing plan, two other interferometers, the “guide” interferometers, observe bright *guide stars* close to the target of interest, to stabilize the orientation of the interferometric baseline. The presence of the two guide interferometers is required for the SIM co-linear architecture, as space-based instruments obviously do not have the benefit (and encumbrances) of a rigidly rotating stable platform from which to operate (the Earth). Thus, to anchor the spacecraft attitude to a celestial coordinates system, guide interferometers lock on two bright reference stars. During the period of time in which SIM baseline is stabilized (~ 1 hr), the science interferometer can observe targets within a 15 degree-diameter Field of Regard (FoR). The area of the sky on which a set of objects is observed with the science interferometer, while the guide interferometers determine the orientation of the science baseline in inertial space, is called a *tile*. Knowledge of the absolute attitude is actually not essential. What matters is that changes in the baseline orientation during the observing period are accurately monitored. The initial length and orientation of the baseline are estimated in the post-processing of the astrometric data.

Global astrometric missions, such as Hipparcos, DIVA, and GAIA, are designed to perform differential angular measurements in their sensitive directions between stars observed at about the same time by centroiding their diffraction-limited images. The basic astrometric observable for SIM is the optical path-length difference between the two arms of the science interferometer, once it is “locked” on the fringes of a target star. The optical path-length delay d_\star can be functionally related to the spacecraft attitude and the three-dimensional instantaneous position on the sky of the target of interest by means of the fundamental astrometric observation equation:

$$d_\star = \mathbf{B} \cdot \mathbf{S}_\star + C + \sigma_\star \quad (1)$$

where $\mathbf{B} = B\mathbf{u}_b$ is the baseline vector of length B , \mathbf{S}_\star is the unit vector to the star being observed, C is a constant term representing residual internal optical path differences, and σ_\star is the single-measurement error on the target position (expressed in picometers). All delay measurements with the science interferometer of objects within the same tile, during the 1 hr observing period, are made with the SIM spacecraft inertially pointed, i.e. while the guide interferometers are used to keep both \mathbf{B} and C constant (at the μas level). The external path delay is determined by means of the introduction of an internal movable delay line, which serves to equalize the optical path-length of the light beams coming from the the right and left arm of the science interferometer to the combination point in the beam combiner. The peak of the interference pattern in the fringe detector occurs when the internal path delay equals the external path delay. The interferometer is sensitive only to the component of the star position that is parallel to the baseline. Thus, each measurement is strictly one-dimensional, in the line defined by the intersection of the plane of the sky and the plane define by the baseline vector and the direction to the star under investigation. The necessary two-dimensional information required to fully determine the position of the object is obtained by making observations with different (possibly orthogonal) orientations of the baseline vector \mathbf{B} .

SIM’s basic set of star measurements happens within a tile with a 15° field. Adjacent tiles overlap each other to establish relative object positions and geometric continuity. Tiles are linked together by stars in the overlap regions, thereby covering the entire sky with a systematic, interlaced brick-work-like pattern of discrete pointings. Within each tile, SIM will observe science targets, but will also observe grid stars. The purposes of the grid stars are to provide links to a global astrometric reference frame, and to determine the attitude of the baseline. The astrometric reference grid, the key to SIM’s wide-angle astrometry, will comprise approximately 3000 stars uniformly distributed on the sky, so that there will be about 10 grid stars per tile, which will be observed together with science targets during the 1-hr observing periods, as well as in dedicated periodic grid observing campaigns. The astrometric grid catalog will have an internal accuracy of $4 \mu\text{as}$, over two orders of magnitude better than the Hipparcos catalog. However, it is with SIM relative (narrow-angle) astrometry that it will be possible to achieve the highest measurement accuracy. SIM’s differential mode will be best suited for science programs where global references are not required, but the highest possible differential performance

is needed, as is the case for the detection of astrometric signatures of planetary companions to nearby stars. The objective of 1 μ as relative astrometry in 1 hr integration time corresponds (see Eq. 1) to an accuracy on the position of the delay line of 50 pm with a 10 m baseline. Relative one-dimensional laser gauge metrology for high-precision measurements and control of changes in baseline length has been demonstrated in laboratories at a level of a few picometers on short time-scales (Gürsel 1993; Noecker 1995; Reasenberg et al. 1995; Leitch et al. 1998), while ongoing three-dimensional experiments at JPL, such as the Micro-Arcsecond Metrology Testbed (Shaklan et al. 1998; Kuhnert et al. 1998), are currently progressing towards the 50 pm goal for SIM (Kuhnert et al. 2000). Finally, the Micro-Precision Interferometer Testbed at JPL has already achieved the 10 nm positional stability requirements on internal optical path-lengths (Neat et al. 1998), necessary to ensure the maintenance of fringe visibility.

While operated in narrow-angle astrometric mode, during an observing period within a single tile, the science interferometer carries out delay measurements of a target star and a number of nearby reference stars, located within a circle ~ 1 degree in diameter, centered on the target. The fundamental measured quantity is then the *relative* delay:

$$\Delta d_{\star,n} = \mathbf{B} \cdot (\mathbf{S}_{\star} - \mathbf{S}_n) + \sigma_d \quad (2)$$

which corresponds to the instantaneous angular distance between the target in the observing plan and its n -th reference star, projected onto the interferometer baseline, while σ_d is the single-measurement accuracy on each relative delay measurement. Note that, to first order, the constant term C cancels out for the set of relative delay measurements within the 1-hr observing period.

3. Simulations of SIM Observations

The simulation and analysis code was developed to perform studies similar to those conducted by Reasenberg et al. (1997), Lattanzi et al. (1997), Sozzetti et al. (2000), and Lattanzi et al. (2000a; 2000b). It has been specifically tailored to reproduce SIM observations in narrow-angle mode.

3.1. Stellar Distribution and Model of Motion

All our simulations use a consistent set of definitions to build a sample of targets with given properties. We start by generating 200 science targets at uniformly-distributed random locations on the celestial sphere. Each defines the center of a circular region (*domain*) of about 1° in diameter, which is the effective field of view for narrow-angle astrometry. Then we generate guide and reference stars for each target. The two guide stars, which ensure the stability of the interferometric baseline during the course of each observation, are placed near the border of each domain, and a predefined number of reference stars is placed randomly within this region. For each

target, reference, and guide star, we express the five basic astrometric parameters (two positions λ and β , two proper motion components μ_λ and μ_β , and parallax π) in ecliptic coordinates. The parallax of the target star is predetermined by each experiment (i.e., the star is placed at a specific distance from the Sun), while the parallax of the reference stars is chosen randomly around 1 mas. Proper motions are generated randomly from a normal distribution with dispersion appropriate to each star—larger for the target, which is assumed to be nearby, and smaller for the more distant reference stars. The introduction of a detailed Galaxy model is a possible future enhancement. However, detectability and measurability of planets are essentially independent of the values of all proper motions and of the parallax of the reference stars. The unperturbed photo-center positions of the target and reference stars are then computed on the basis of the five astrometric parameters of each star. Then, we correct the photo-center position of the target for the gravitational perturbation induced by the presence of a planetary mass companion. The Keplerian motion of the orbiting planet is described via the full set of seven orbital parameters: semi-major axis a , period T , eccentricity e , inclination i , longitude of pericenter ω , position angle of the line of nodes Ω , and epoch of pericenter passage τ . The target’s actual orbital motion around the system barycenter is then obtained by scaling the planet’s semi-major axis by the ratio of masses and the distance.

To describe the target motion on the celestial sphere, we have adopted a linear analytic model, in which the difference between the position vector to the target \mathbf{S}_\star evaluated at time t and the same quantity \mathbf{S}'_\star measured at time t' is expressed as a sum of small perturbative terms to the initial location of the target on the sky, due to proper motion, parallax, and the gravitational perturbation induced by the orbiting planet:

$$\mathbf{S}'_\star - \mathbf{S}_\star = d\mathbf{S}_\star = d\mathbf{S}_\mu + d\mathbf{S}_\pi + d\mathbf{S}_K \quad (3)$$

In this model, second order effects such as relativistic aberration and light deflection from the major solar-system bodies are not taken into account, nor have we considered other secular changes in the target’s position due for example to changing proper motion (perspective acceleration) or changing parallax. Realistically, such effects will have to be taken in consideration in future experiments. However, in these studies we assume that *a-priori* corrections for higher order effects have been made to the simulated observations which we use as input to the detection and analysis part of the code. Also, targets and reference stars are assumed astrometrically clean: sources of astrometric noise such as flares or spots on the stellar surface have not been modeled throughout our simulations, nor have we discussed the possibility of binaries among either targets or reference stars, except for the single planet orbiting the target star.

Finally, we generate a set of narrow-angle observations of each system at predefined times and baseline orientations, adding measurement errors as discussed below.

3.2. Error Model and Observing Scenario

Currently, SIM narrow angle error budget for each one-dimensional visit assumes that a $1 \mu\text{as}$ accuracy on one axis will be reached for both target and reference stars, with errors scaling as the square root of the exposure time \sqrt{t} , after a nominal 1 hr “performance specification period”, which comprises spacecraft slewing between adjacent wide-angle FoRs, stabilization and acquisition of two bright guide stars in order to allow the instrument to maintain the correct attitude during observations within that FoR, observations of a number of grid stars, which are used to remove instrumental thermal drifts, and sequences of elemental fringe measurements of the target and its reference stars, which are called *unit observing blocks*. Within each unit observing block, the science interferometer executes elemental delay measurements of the target and reference stars in turn, with a minimum integration time per object of 30 sec, needed for metrology stabilization. The effect of thermal drifts is such that the maximum duration of each observing block is currently constrained to be no greater than 5 minutes, even if a thorough understanding of the tradeoff between longer integration times (and increased efficiency) and possible performance degradation with longer time-scales has not yet been achieved.

At present, knowledge of error sources aboard SIM is still incomplete, nevertheless it is possible to summarize the error contribution to narrow-angle astrometric measurements as composed of two parts, a photon noise component and an instrument systematic component: the former is mainly a measure of instrument throughput, including for example contributions from detector quantum efficiency, mirror reflectivity, and imperfect fringe visibility; the latter represents the sum of known and estimated contributions to the optical path difference (delay) which are instrumental in origin. The system noise and photon response contribute to the single-measurement accuracy as (see for example the official SIM website, <http://sim.jpl.nasa.gov>, and documentation therein):

$$\sigma = \sqrt{\sigma_{\text{sist}}^2 + \sigma_{\text{phot}}^2 \times 10^{\frac{V-V_0}{2.5}} \times (t_0/t)} \quad (4)$$

where a reference photon sensitivity $\sigma_{\text{phot}} = 4 \mu\text{as}$ is reached in $t_0 = 14.1$ hr for a star of magnitude $V_0 = 20$ mag. For a system noise $\sigma_{\text{sist}} = 1.718 \mu\text{as}$, and for a target and reference stars brighter than $V = 11$ mag, in $t = 30$ sec integration time it is possible to achieve an astrometric accuracy of $3 \mu\text{as}$ on each object. In principle, at the end of 10 unit observing blocks a $1 \mu\text{as}$ precision is reached on one axis, for each object. This simplified noise model does not account for any term with an explicit dependence on the angle to the reference star ϑ_{R} . This error is due to the so-called “beam walk”, as the delay line is slewed and the siderostat is rotated, and is expected to grow linearly with ϑ_{R} .

In this exploratory study we have implemented a simplified observational scenario, in which n reference stars are initially placed around each target within the 1° domain. A one-dimensional observation, which we will call *Standard Visit* hereafter, consists of a sequence of elemental fringe measurements by the science interferometer of a target star and its reference stars, while the two pointing interferometers are locked onto the bright guide stars. In reality, observations of grid stars

(4 at least) should be executed at the beginning and end of the Standard Visit to measure the size and orientation of the baseline with the needed accuracy. For the moment, we do not include grid stars observations in our simulations, and assume the orientation and length of the interferometric baseline are perfectly known. The structure of each standard visit is then defined as follows. We carry out N_b unit observing blocks (not to exceed the 1-hr “performance specification period”), each composed of n 30-sec measurements of the target and one 30-sec measurement for each of the n reference objects. Assuming a typical 30-sec repositioning time, each unit observing block lasts $30 \times n + 30 \times n + 2 \times 30 \times n \text{ sec} = 2 \times n \text{ minutes}$. We satisfy the underlying constraint of 5 minutes limit duration of each set of measurements of target and reference stars, due to thermal drifts, in that each pair of target/reference star elemental fringe measurement is completed in only 2 minutes. The Standard Visit can thus be regarded as a sequence of n *differential* measurements between the target and each of the n reference stars, of the form: $T_1 - R_1, T_2 - R_2, \dots, T_n - R_n$.

If we assume independent errors in the measured positions of target and reference stars (in our present analysis we do not account for possible correlations), then at the end of each one-dimensional Standard Visit the single-measurement error σ_d on each of the n relative delays will be:

$$\sigma_d = \frac{\sqrt{\sigma_{*,n}^2 + \sigma_{R,n}^2}}{\sqrt{N_b}} \quad (5)$$

with $\sigma_{*,n}$ and $\sigma_{R,n}$ the elemental fringe measurement errors on each object defined by Eq. 4. Assuming the target and its n reference stars are bright ($V \leq 11$), then for each 30-sec elemental fringe measurement we obtain $\sigma_{*,n} = \sigma_{R,n} = 3 \mu\text{as}$. Finally, we set $N_b = 4$, thus each of the n differential measurements at the end of a Standard Visit (from Eq. 5) has an error $\sigma_d \simeq 2 \mu\text{as}$. We will refer to the *relative* delay accuracy σ_d as the Standard Visit accuracy throughout the rest of this paper.

Standard Visits of targets and reference stars can be made at arbitrary times and arbitrary spacecraft orientations, throughout the 5-year nominal mission lifetime—we neglect at this point possible visibility, orientation, and planning constraints that might restrict the observing sequence⁶. Each visit is strictly composed of one-dimensional measurements, then additional observations with orthogonal orientations of the baseline are required. Thus, we define a *full two-dimensional astrometric observation* as the sum of two (one-dimensional) Standard Visits executed with baselines at approximately right angles with each other. The time separation between pairs of Standard Visits is chosen randomly between 0 and 5 days.

⁶The SIM spacecraft is currently supposed to be operated in an Earth-trailing orbit, thus avoiding Earth’s occultations that would occur in a low-Earth orbit. Only a Sun exclusion angle (presently set to 43°) will introduce restrictions on the observing schedule. The Sun exclusion zone will primarily affect the periodic grid observing campaigns, for which different scenarios have been evaluated. The possible impact of the Sun exclusion zone on actual observing strategies for science targets and the limitations it may impose on the detectability of planets with a given period will ultimately be assessed only after a definite choice for the grid observing campaigns has been made

4. Data Analysis Methods

This section outlines the data analysis procedure we have developed and implemented in the analysis part of the code to assess SIM’s ability to discover and measure planets. For each case, planet detectability is measured via a standard χ^2 test of the null hypothesis that there is no planet. If deviations in the observation residuals exceed a predefined significance threshold, then the planet is considered detected, and its orbit is determined by a full non-linear least-squares fit to the observed relative delay measurements. The fit also determines the relative positions, proper motions, and parallaxes of target and reference stars, which are of course not known *a priori*. We derive errors in the measured orbital parameters empirically, by comparison of the values determined from the fit with the true (input) values.

4.1. Planet Detection

To determine planet detectability, we conduct a null test: we *assume* that the target is a single star with no companions, and determine whether (and with what confidence) this assumption can be proven false. This process has two steps: first, determine the astrometric parameters of target and reference stars under the no-planet assumption; second, compute the discrepancy between the best no-planet solution and the actual measurements. A detectable planet will cause a statistically significant discrepancy.

Since all measurements are differential, positions, proper motions, and parallaxes of target and reference stars are not fully constrained by the time series of measured delays. Specifically, the least squares problem has a rank deficiency of 5, corresponding to the five parameters that cannot be determined by the observations: two position zero points, two proper motions zero points, and a parallax zero point (in the narrow-angle approximation). A convenient solution is to choose a so-called *base object* among the set of reference stars, and to hold its astrometric parameters fixed at their starting values throughout the fitting procedure. Then, astrometric parameters of all other objects are measured relatively to those for the base object. This approximation may break down for sufficiently large parallaxes and field angles, since parallaxes at different places in the sky are not exactly additive. However, as long as an approximate *absolute* parallax can be determined from the grid solution, we expect the errors introduced by this approximation to be negligible.

If the position of the target star is perturbed by a planet, the resulting no-planet solution will have post-fit residuals large compared with observational noise. These observation residuals will contain systematic deviations due to the companion. A simple way of assessing planet detectability is to apply a standard χ^2 test to the residuals of the single-star fit, assuming that the uncertainties of the individual measurements are known. We compute the probability $P(\chi^2 \geq \chi_o^2)$ of obtaining χ^2 greater or equal to that observed (χ_o^2), assuming the single-star model to be correct: if such probability is greater than a given threshold, the *acceptance level*, then the observations are

consistent with the assumption of no orbital motion; if P drops below the acceptance level, then the single-star model is rejected, and the planet is considered detected at the corresponding confidence level. We set an acceptance level of 5% – and a corresponding confidence level of 95% – throughout our simulations. By definition, this method only measures significant deviations from an *a priori* model, and does not provide elements for a direct identification of the nature of the observation residuals. To this end, residuals are usually inspected by means of standard periodogram analyses. In our simplified scenario, the star+planet model fits the data well and therefore the planet can be considered detected (later on in Section 5.2.1 we provide quantitative examples). However, in more realistic circumstances, the relative quality of the single-star and star+planet fits should be compared, and a statistical test applied to determine the true significance of the detection. Furthermore, the level of detection threshold in the presence of real-world disturbances can be a source of concern. Indeed, the 95% confidence level which was adopted in our tests may well be too liberal to indicate detection in the presence of realistic astrophysical and instrumental noise. A realistic threshold for truly reliable detection can only be established once a more complete model of instrumental and astrophysical effects is available. In the context of this exploratory study, we choose a confidence level of 95% because it leads to manageable numerical experiments. We will discuss possible enhancements in planet detection methods in a future work.

4.2. Orbit Determination

Once a planet is detected, the goal is to determine its orbital characteristics and mass. We therefore expand our fitting procedure to allow for the presence of a planet around the target star. The photo-center motion of the target includes the gravitational perturbations due to a planet, whose seven Keplerian elements—which fully describe its orbital motion—are added to the list of unknowns to be determined. In evaluating the observation residuals, we employ an analytic model in which the computed relative delay between the target and its n -th reference star is in the form:

$$\Delta d_{*,n} = \mathbf{B} \cdot (\mathbf{S}_*(\lambda_*, \beta_*, \mu_{\lambda,*}, \mu_{\beta,*}, \pi_*, X_1, X_2, X_3, X_4, e, T, \tau) - \mathbf{S}_n(\lambda_n, \beta_n, \mu_{\lambda,n}, \mu_{\beta,n}, \pi_n)) \quad (6)$$

For convenience, we use the Thiele-Innes representation of the orbital parameters, in which a , i , ω , and Ω are combined to form the four Thiele-Innes elements X_i , $i = 1, \dots, 4$ (see for example Green (1985)). The Thiele-Innes representation is better behaved for fitting purposes, as it reduces to three the number of non-linear parameters in the observation equations, thus improving the convergence speed of the iterative least squares algorithm. At the end of the simulation, the classic orbital parameters are recomputed from the Thiele-Innes elements.

Note that the mass of the planet is *not* determined directly from the orbital parameters. In fact, the planet mass can only be determined if an independent estimate of the mass of the parent

star is available, for example, from its spectral and luminosity class. The mass of the orbiting planet would then be computed via the mass function formula:

$$\frac{M_p^3}{(M_\star + M_p)^2} = \frac{a_\star^3}{\pi^3} \frac{1}{T^2} \quad (7)$$

where M_p and M_\star are the planetary and stellar mass in solar-mass units, T the orbital period in years, π the parallax and a_\star the semi-major axis of the orbit of the central star around the barycenter, both expressed in arcsec. The fit to the observed relative delays determines a_\star , π , and T directly, while M_p can be computed if M_\star is known or estimated. In fact, under the reasonable assumption $M_p \ll M_\star$, we can then derive the planet mass via the following approximate formula:

$$M_p \simeq \left(\frac{a_\star^3}{\pi^3} \frac{M_\star^2}{T^2} \right)^{1/3} \quad (8)$$

4.2.1. Initial parameters

We have implemented an iterative method for the solution of the highly non-linear system of equations of condition that utilizes the Levenberg-Marquardt algorithm (Press et al. 1992). Initial guesses for the unknown parameters are needed to start the fitting process. The solution at step k is updated with respect to the solution at step $k - 1$, then the variable χ^2 (i.e., the sum of the square of the observation residuals) is checked for convergence of the solution: if $\Delta\chi^2 = \chi_{k-1}^2 - \chi_k^2 \leq 0.01$, iterations are stopped. A natural choice of the condition for stopping iterations consists of requiring that χ^2 *decreases* by a negligible amount, absolute or fractional (if the opposite behavior is observed, then further iterations are necessary for stabilization of the solution). As a matter of fact, because the minimum of χ^2 is at best only a statistical estimate of the fitted parameters, a variation in the parameters that changes χ^2 by a quantity $\ll 1$ is generally not statistically meaningful, as with this method the parameters, once they approach the configuration which minimizes the fitted function, tend to wander around in the vicinity of the minimum, in a flat valley of complicated topology.

In any iterative, non-linear fitting procedure, the choice of the initial guess for the unknown parameters can have a significant impact on the convergence of the method and the quality of the solution, especially because of the possibility of false (local) minima of the χ^2 function. Unlike Konacki et al. (2002), since we are focusing primarily on the performance that SIM can ultimately achieve in detecting and measuring planets, the orbital fitting results we discuss in the next section used *good* guesses, which means they were obtained with initial guesses differing from the “known” values of each parameter by only a moderate amount of noise. The deviations of the resulting fitted parameters from their true values should then be a useful measure of the accuracy in orbit reconstruction that can ultimately be achieved with the assumed measurement errors. Note also that our detection estimates are intrinsically independent of the choice of initial parameters,

since the detection least squares problem is linear in all fitted parameters (in the narrow-angle approximation), and therefore its solution is independent of the initial parameters.

Nevertheless, a proper assessment of the effectiveness of any overall search and measurement strategy requires a more realistic approach. Initial parameters must be determined solely on the basis of the actual measurements, without any *a priori* knowledge of the system, and double-blind tests must be conducted to verify the global performance of the search and analysis method. Work is in progress, and will be presented in the future, on refined models for global search and optimization strategies of starting guesses for orbital parameters, where we take into account the results from standard periodogram analysis as well as detailed Fourier analyses of the astrometric signal.

5. Results

The observation-modeling and analysis software we have developed have allowed us to provide a first quantitative estimation of the ability of SIM to detect and characterize the orbits of planets around nearby stars. Preliminary findings were shown by Casertano & Sozzetti (1999). The more general and complete set of results we present in this Section has been obtained using a number of *a priori* assumptions (see Sections 3 and 4) on the instrument (perfect knowledge of the error model and of the satellite attitude), on the systems to be investigated (astrometrically clean targets and reference stars, no stellar companions, single planets), and on the data analysis procedures (avoiding studies of periodicities and double-blind tests, and utilizing good guesses for the values of the orbital parameters necessary to initialize the least squares solution). The main focus of this work is on the goal of determining SIM’s *ultimate* ability to detect and measure single planets around single, normal, nearby stars, and the above assumptions constitute the most efficient way to achieve it. We expect that some of these assumptions will have a non-negligible impact on the actual planet-finding capabilities of SIM, which should be revisited when a more realistic description of the satellite and its operations becomes available.

In this Section, we present and discuss our most significant results, as follows. First, we compute detection probabilities and estimate the accuracy achievable in measuring the orbital elements and mass of a planet as a function of its characteristics and of SIM single-measurement precision, utilizing a template observing strategy based on the simplified observational scenario sketched in Section 3. Next, we study the performance of different observing strategies, varying the number and time-spacing of observations, and the number of available reference stars around the target. Finally, we discuss the merit of more flexible observing scenarios to be applied to both bright ($V \leq 11$) and faint targets, and utilize them to identify the boundaries of the discovery space of SIM for detection of terrestrial planets around a sample of the nearest solar-type stars and M dwarfs.

5.1. Detection Probabilities

Astrometric observations of a star contain its reflex motion due to orbiting bodies, including planets. The apparent magnitude of this perturbation, the orbital motion of the star around the center of mass of the system, is the so-called *astrometric signature*:

$$\alpha = \frac{M_p a_p}{M_\star D}, \quad (9)$$

where M_p and M_\star are, respectively, the mass of the planet and the central star, a_p is the semi-major axis of the planet’s orbit, and D the distance of the system from the observer. If M_p and M_\star are given in solar mass units, a_p in AU, and D in parsec, then α is in arcsec.

In principle, detection probability will depend upon *a*) measurement errors due to correlated and uncorrelated instrumental and astrophysical noise sources, *b*) mission parameters, and *c*) distance and properties of the observed star-planet systems. We have discussed in section 3 and 4 the basic assumptions we have made while taking into account the contributions to points *a*) and *b*). As for point *c*), we will express detection probabilities as function of the orbital period T of the planet, the distance D from the observer, and the astrometric signature α . In particular, our simulations are based on an assumed Standard Visit accuracy $\sigma_d = 2 \mu\text{as}$ for each relative delay measurement, which applies to bright targets and reference stars ($V \leq 11$ mag), in the context of the current best-estimate error budget for SIM narrow-angle astrometric observations, and for a structure of the Standard Visit as discussed in Section 3.2. In order to apply our results to a different single-measurement accuracy, we note that the detection probability depends on α and σ_d only through their ratio, which we call the “scaled signal”:

$$S = \alpha/\sigma_d \quad (10)$$

Similar scaling applies to the precision with which the orbital parameters can be determined. Thus, the results we present here can be easily rescaled to different measurement errors. For given scaled signal, the detection probability depends, of course, on all other orbital parameters, and especially on the period T of the orbit.

First of all, we ran a set of simulations without planets, generating spheres of 200 uniformly distributed targets, and observed them with a template observing strategy, in which a specified number of reference objects is chosen for each target, together with a fixed number and time-spacing of pairs of one-dimensional orthogonal observations, during the nominal mission duration. For the purpose of our analysis, we have placed $N_r = 3$ astrometrically clean reference stars within a 1° domain centered around each target, and adopted sequences of $N_o = 24$ two-dimensional (orthogonal) narrow-angle observations (as defined in Section 3.2) equally spaced over the 5-yr mission duration, with a time interval between pairs of successive observations fixed to 0.2 years, and assuming that a full observation is completed within 5 days. We thus have a total of $N_m = 144$ relative delay measurements, and a total of $N_p = 20$ unknown parameters to solve for in the set of observation equations, i.e. five astrometric parameters for the target and each of the components

of its local reference frame. Within this template observational scenario, a Standard Visit lasts about half an hour, well within the recommended 1-hr limit. The observing sequence described above was utilized to obtain all simulation results discussed in this and the following section. We have verified the correct behavior of the χ^2 test and the choice of the confidence level, as described in the previous Section. As expected, the number of *false detections* was $\simeq 5\%$. Then, we have used the χ^2 test to analyze 320 000 $1-M_\odot$ stars uniformly distributed on the sky, orbited by single planets producing astrometric signatures in the range $1 \leq \alpha \leq 40 \mu\text{as}$, with periods in the range $0.5 \leq T \leq 20 \text{ yr}$. We averaged over the remaining orbital elements, distributed randomly in the ranges: $0^\circ \leq i \leq 90^\circ$, $0 \leq e \leq 1$, $0 \leq \Omega \leq \pi$, $0 \leq \omega \leq 2\pi$, $0 \leq \tau \leq T$.

Figure 1 summarizes the main characteristics of the planet detection probability. As discussed above, we consider a planet detected when the null-test, based on the χ^2 of the astrometric solution for target and reference stars assuming that there is no planet, fails at the 95% confidence level. The curves in Figure 1 represent equal probability contours for the detection; thus, for example the curve marked 95% indicates the locus of the period T and scaled signal S for which 95% of the planets generated in our simulations fail the null-test, at the 95% confidence level. The minimum astrometric signature required to achieve secure detection must be $\alpha_{\text{min}} \sim 2.2$ times the Standard Visit accuracy σ_d (we recall that accuracy refers to independent measurements of relative delays between the target and each of its reference stars), for periods between 0.5 and 5 years. Due to the increasingly worse orbital sampling, the required signal rises sharply for periods longer than the mission length, especially for high detection probabilities. However, a Jupiter-Sun system, with a period of 11.8 years, can still be detected 50% of the time if the astrometric signature is about $4\sigma_d$, or to a distance of 500 pc.

The dashed lines indicate the signature produced by systems composed of a $1-M_\odot$ primary and a $20-M_\oplus$ planet placed at the distance shown in the legend, as a function of orbital period (in parentheses, the equivalent distance at which a system composed of a solar-mass star and Jupiter-mass planet would produce the same signature). These curves are derived by substituting Kepler’s third law in the defining expression for α (Eq. 9), in the limit for $M_p \ll M_\star$:

$$\alpha \simeq \frac{M_p}{M_\star^{2/3}} \frac{T^{2/3}}{D} \quad (11)$$

Thus, for example, a Jupiter-mass planet at 300 pc (long-dashed lines), or equivalently a Neptune-class planet placed at 20 pc, can be detected with 95% probability around a $1-M_\odot$ star if its orbital period is roughly between 1.5 and 8.5 years—the range over which the long-dashed line lies above the 95% contour.

A different representation of the same results is shown in Figure 2, where the isoprobability contours are drawn as function of the period and distance, for a Jupiter-mass planet around a solar-mass star. The maximum detection distance peaks for $T \simeq 4$ years; shorter periods correspond to smaller orbital amplitudes, and thus smaller values of S , while planets with longer periods suffer from increasingly incomplete orbital sampling.

In Figure 3 we show the behavior of the detection probability as function of S , for different orbital periods. As already emphasized by Reasenberg et al. (1997) and Lattanzi et al. (2000a), who studied the planet-finding capabilities of the proposed NASA mission POINTS and of the recently approved ESA Cornerstone Mission GAIA, planets with periods longer than the mission lifetime require a much stronger signal in order to be detected with high confidence. Finally, this plot highlights how, within the range of favorable periods ($0.5 \leq T \leq 5$ yr), detectability in the case of $T = 1$ year (dashed-dotted-dotted line) is slightly affected by the coupling between orbital and parallactic motion.

5.2. Estimation of Planet Mass and Orbital Elements

Just as the detection probability (for a given choice of the observing strategy), the ability in measuring accurately the set of orbital parameters for a detected planetary system is closely related to the period and the astrometric signature induced by the unseen planet on the observed parent star.

First, we have utilized our simplified but realistic observational scenario to provide an estimate of the rms errors expected on the determination of orbital parameters and masses in a handful of significant cases, together with an evaluation of the quality of fits that may be obtained. Next, we have determined the boundaries, in the $\alpha - T$ plane, of SIM ability to accurately determine the orbital geometry and mass of a single planet orbiting a single normal nearby star, by evaluating the minimum astrometric signature required for measurements of a given orbital parameter or the mass of the planet good to a given accuracy level. Finally, we have considered how the presently known candidate planets would fall within the limits of SIM’s detection and orbit reconstruction capabilities. The extra-solar planets found so far constitute a natural laboratory for conducting physical studies of planetary systems with SIM. In fact, astrometry measures two projections of an orbit, as opposed to the intrinsically one-dimensional radial-velocity measurements, and thus can determine the entire set of 7 orbital parameters. To this end, SIM’s highly accurate measurements will be instrumental in breaking the inclination degeneracy intrinsic to radial velocity observations, and this will allow in turn a direct estimate of a planet’s true mass. As discussed in detail below, M_p and i are two key parameters to be determined for a proper understanding of the nature and diversity of sub-stellar companions.

5.2.1. Empirical Errors and Quality of Fits

Our simulations cover four particularly significant cases: 1) a Jupiter-mass planet in orbit around a solar-mass star with $T = 1$ year at $D = 100$ pc, to quantify the effect of the coupling between parallactic factor and orbital period when attempting the orbit reconstruction; 2) the same system but with an orbital period $T = 5$ years at $D = 200$ pc, in an almost ideal configuration

where the orbital period equals the mission duration; 3) a short-period ($T = 15$ days) giant planet ($M = 4 M_J$) around a $1-M_\odot$ at $D = 30$ pc, to test SIM’s ability to cope with poorly sampled motion; 4) a “true” Jupiter-Sun system, with a period of 12 years—over twice the mission duration—at $D = 100$ pc, to stretch SIM’s ability to solve long-period orbits. These four systems have scaled signals $S = 5, 7, 8,$ and $25,$ respectively.

In all cases, utilizing the template observing scenario described in Sections 3.2 and 5.1, we have simulated SIM observations of 200 systems uniformly distributed on the sphere, averaging over the remaining orbital parameters ($i, e, \tau, \omega,$ and Ω). We have then modeled a single-star fit on the simulated observations, and in all cases excessive residuals indicated (with a 95% confidence level) the presence of a companion. Finally, we fitted the measured perturbation of the unseen secondary with a full Keplerian orbit. The deviation of the fitted parameters from their true values gives an indication of the accuracy of the measurements. The results for three of the four cases mentioned above are presented in Figure 4. For each parameter, the rms deviation of measured from true value is given in its respective panel.

The general indication is that a scaled signal $S \simeq 5$ (minimum astrometric signature 5 times larger than the single-measurement precision) is sufficient to measure the parameters of the system with an rms error of about 20-30%, as long as at least one entire orbit is observed during the mission lifetime. If $T > 5$ yr, a stronger signal is required, and the error distribution can have an enhanced tail, particularly in the case of the semi-major axis a , because of systems which, due to eccentricity, orientation, and phase, have an unfavorable orbital sampling during the time spanned by the observations. Due to the good orbital sampling, the 1-yr period is recovered very accurately, and the coupling between parallactic and orbital motion (highlighted by the broader distribution of rms errors on π) turns out to have a less critical impact than one might have anticipated.

Simulations of a giant planet in a very fast orbit around a $1-M_\odot$ star at $D = 30$ pc are not shown in the figure, as no reliable orbit can be obtained for this system. The planet can be clearly detected in the observation residuals, but the 0.2-yr sampling period is larger than the very short orbital period ($T \simeq 15$ days), and aliasing effects cause the orbital fit to be poorly constrained. As we discuss later on in Section 5.3, for detectable planets in very fast orbits reliable orbital fits will likely require the adoption of *ad hoc* strategies in the distribution of the observations, to ensure proper coverage of the short periodicity of the signal.

In Figures 5 and 6 we present graphical illustrations of the quality of the fits that can be obtained for star-planet systems, in the most favorable case among the four discussed above. Specifically, the two Figures show information for the system composed of a $1-M_\odot$ star and a $1-M_J$ planet placed at $D = 200$ pc, with the planet in a 5-yr period, eccentric ($e = 0.6$) orbit, and with the orbital plane inclined of an angle $i = 45^\circ$ with respect to the line of sight. The panels in Figure 5 show the apparent motion in the plane of the sky, and the residuals of the single-star fit. The apparent motion is dominated by the proper motion and parallax of the primary (along both

the X- and Y-axis), and the motion due to the planet cannot be discerned in these full-scale plots. The observation residuals after proper motion and parallax have been subtracted still highlight significant scatter, up to over 5 times the Standard Visit accuracy ($\sigma_d = 2 \mu\text{as}$). The panels in Figure 6 show the residual motion, measured and fitted, after subtraction of the best-fit proper motion and parallax terms, thus displaying more clearly the effect of the planet. After a fully Keplerian orbit is modeled on the observations, the residuals exhibit a scatter no larger than $\sim 2\sigma_d$, consistent with the absence of further companions, at the level of the single-measurement error. In particular, in the lower right panel we can appreciate a slight offset (in both X- and Y-axis) of at most 2-3 μas between the true and the post-fit reconstructed orbital motion, in agreement with the residual scatter observed in the post-fit residuals, and to be compared with the analog rms error on the semi-major axis shown in the upper right panel of Figure 4.

5.2.2. Accurate Orbit Reconstruction and Measurement of Known Planets

To provide an overall estimate of SIM’s ultimate capability in measuring single planets around single, nearby solar-type stars, we follow the same logic adopted in Section 5.1, in which we discussed isoprobability curves for 95% confidence of detection. A minimum astrometric signature $\alpha_{\min} \sim 2.2\sigma_d$ was required for secure detection, for periods shorter than the mission lifetime, with a sharp rise in the required signal for $T > 5$ years. Similarly, it is possible to define the minimum astrometric signature required for measurements of a given orbital parameter or the mass of the planet good to a given accuracy level. We ran simulations adopting the same observational scenario described in Section 5.1, but letting astrometric signatures vary in the range $1 \leq \alpha \leq 1000 \mu\text{as}$. We have then obtained the “probability of convergence” for the orbital parameters and mass of the planet, i.e. the percentage of the values for each parameter that in a simulation, after modeling the observations with a full Keplerian orbit, falls within a given fraction of the true value. The criterion for stopping the iterative fitting procedure is the one described in Section 4.2.1. Similarly to Section 5.1, we assume a given orbital element is confidently estimated with, say, 30% accuracy if the relative convergence probability within the same fraction of the true value is $\geq 95\%$. We find that, for example, for periods shorter than the mission length, mass measurements accurate to 10% require $\alpha \simeq 10\alpha_{\min}$, and to measure the inclination at the same level of accuracy we need a stronger signal, $\alpha \simeq 15\alpha_{\min}$. The other orbital elements (e , τ , ω , and Ω) are accurately determined when the astrometric signature $\alpha \simeq 5 - 15\alpha_{\min}$, while depending on how many orbits are fully sampled, the period T can be estimated with higher accuracy at smaller values of α .

The limits in SIM’s ability to detect and measure planets are better understood in terms of: 1) the impact of its measurements on future planet discoveries, and 2) the wealth of information its high-precision astrometric observations will provide for a complete classification of planetary systems. Figure 7 shows how, in the plane $\alpha - T$, the set of presently known candidate planets falls within the boundaries for secure detection and accurate orbit and mass determination with SIM discussed in Section 5.1 and above. We focus in particular on the accurate measurement

of M_p and i , as high-precision astrometry contributes decisively to the complete determination of the true orbit of a planet by removing the inclination degeneracy intrinsic to radial velocity measurements, thus providing a direct estimate of its true mass. In Figure 7, the known planet candidates are plotted for the worst case when the orbit is viewed edge-on. The ‘worst case’ means that the true mass and true astrometric signature equal their radial-velocity minimum values. The real performance on most planets will improve, as depending on the actual inclination angles, the true masses and astrometric signatures will be stronger than plotted. For example, if the currently unknown inclination angle of HD 177830 is found to be 45° , instead of 90° as assumed for the plot, the mass of the planet is 1.4 times larger than the minimum mass determined by spectroscopy ($1.8 M_J$ instead of $1.28 M_J$). The expected uncertainty of our mass determination is an absolute mass which we express as a percentage—22% in this case—of the minimum mass. Thus, in this example, while the uncertainty in the true mass remains essentially unchanged at $0.28 M_J$, the fractional error improves to 16% of the planet mass, instead of 22%.

As a general result, within the limits of the simplified observational scenario sketched in Sections 3.2 and 5.1, we find that $\sim 75\%$ of the present-day known planets would be detected by SIM, and $\sim 50\%$ of them would have mass and inclination of the orbital plane measured to 10% accuracy or better. Independent and accurate estimates of the true masses *and* inclination angles of the planet candidates will provide important information that will help move in the direction of a thorough understanding of the nature of such sub-stellar companions. In fact, today there is still a lack of common consensus on the definition criteria of planets and brown dwarfs, and mass alone may not be sufficient in order to establish whether a low mass companion to a star is a planet, unless its mass is close to that of the Earth (Black 1997). For example, some of the present planet candidates have minimum masses close to the (somewhat artificial) $13 M_J$ dividing line between the two classes of objects set by the no-deuterium burning argument, and might end up belonging to the latter class (due to the actual values of the inclination angles). On the other hand, depending on whether planets and brown dwarfs will turn out to be formed by different or similar mechanisms, the $13 M_J$ cut-off itself might constitute a poor basis for classification. Indeed, we might discover that planets and brown dwarfs share a common mass-range. For a complete comprehension of the nature and diversity of sub-stellar companions, other genesis indicators will have to be evaluated, such as orbit shape and alignment of orbits in multiple systems, or composition and thermal structure of the atmospheres.

A closer look at Figure 7 shows that, for example, the two outer planets (*v* And c and *v* And d) in the three-planet system around the star *v* Andromedæ (Butler et al. 1999) would both have mass and inclination of the respective orbital planes measured with high accuracy, while the signal due to the presence of the innermost planet is not even detectable. As for the other candidate planetary systems, in all cases at least one of the planets is measured with high accuracy (10% or better). Then, the question arises naturally. Could SIM establish, and with which accuracy, whether planets in a planetary system lie on coplanar orbits, or not? The unexpected orbital arrangement of the planets orbiting *v* Andromedæ has for example triggered an on-going debate

on the system architecture, orbital evolution and long-term stability (Laughlin & Adams 1999; Rivera & Lissauer 2000; Stepinski et al. 2000; Barnes & Quinn 2000). Then, determining the actual planet masses *and* three-dimensional geometry of the system becomes crucial in order for theory to derive sensible conclusions on such issues. In paper II, we will present results from extensive simulations of SIM observations of extra-solar multiple-planet systems, in order to quantify SIM’s capability to discover and measure systems of planets, as well as detailed studies of SIM ability to determine coplanarity of multiple-planet orbits. Following similar, recent analyses (Sozzetti et al. 2001), we will show how, by accurately measuring inclination angles and lines of nodes in multiple-planet systems, SIM will provide important observational data which will help learn about the dynamics of evolution of planetary systems, as well as contribute to the understanding of the intrinsic nature of sub-stellar companions.

5.3. Observing Strategy Analysis

The results presented in Section 5.1 and 5.2 constitute a first step towards a proper assessment of SIM detection sensitivity and ability to accurately determine the full three-dimensional orbital geometry and the mass of single planets orbiting single nearby solar-type stars. Our findings have been expressed as function of: *a*) the most relevant physical and dynamical parameters of the observed systems (mass, distance, orbital period), and *b*) the most basic instrument characteristics. In particular, we utilized a simplified, but realistic, observational scenario (see Section 3.2 and 5.1), in which we kept *fixed* the number of reference stars and the number and time-spacing of full two-dimensional observations during the mission duration. These results apply to bright targets and reference stars ($V \leq 11$), in the context of a simple model of SIM elemental fringe measurement error (see Section 3.2), expressed in terms of the visual magnitude and the integration time on the measured object.

In reality, the overall scientific performance of SIM operated in narrow-angle mode, both in terms of 1) its potential for unprecedented discoveries, and 2) its capability to accurately measure crucial parameters (masses, inclination of orbital planes) for a better understanding of planet formation and evolution processes, will be optimized only by implementing flexible observing strategies, sometimes specifically tailored to a single target, to maximize the ratio of the number and intrinsic scientific interest of the objects in the target list to the fraction of the total observing time utilized.

In this Section we analyze the performances of different observing strategies as function of the number of reference stars per target, the total number of full (two-dimensional) observations, the time-spacing of epochs at which Standard Visits are executed, and the structure of the Standard Visit itself, to account for both bright and faint targets. This will allow us to identify a more flexible observational scenario, which we will use in Section 5.4 to delineate the borders of SIM discovery space for detection of Earth-class planets around the closest stars.

5.3.1. Number of observations and reference stars

The robustness of the local reference frame relative to which a target position is measured crucially depends on the availability of a sufficient number of clean reference stars, for which all possible astrophysical astrometric noise sources (such as binarity and surface activity) are either well certified, or negligible at the μas level. It is conceivable that astrometrically clean reference objects will be carefully selected for targets in narrow-angle mode before SIM’s launch by accurate preparatory ground based spectroscopic work; however, it is possible that one or more of the selected reference stars for a given science object might turn out to be not astrometrically stable at the level required for very precise local astrometry. In some cases such ill-behaved objects might have to be removed from the local reference frame. In the event of anomalies discovered in individual reference stars, it would be beneficial if their number (wherever it would be feasible) was sufficiently high right from the start of SIM observations, to increase the robustness of the local frame of reference. This in turn means more unknowns to be solved for (five more for each reference object), so in principle more observations are needed to guarantee the same performance in terms of detectability and measurability of planets.

To verify which scaling applies to detection sensitivity and accuracy in orbit reconstruction and mass determination in the case of a change *a*) in the number of reference stars per target N_r , or *b*) in the number of full observations N_o during the 5 yr mission, we have simulated uniform spheres of 200 Jupiter-Sun systems, with orbital period $T = 5$ yr, near the peak in the detection probability curve in Figure 2, and averaged over the remaining orbital parameters.

For a Standard Visit accuracy $\sigma_d = 2 \mu\text{as}$ on each relative delay, Figure 8 shows the maximum distance at which, for the system described above, detection probability $P \geq 95\%$, as a function of the number of two-dimensional equally-spaced observations, and for 3 and 6 astrometrically clean reference stars, respectively. As expected for a situation in which single-measurement errors are independent, we verify a simple scaling in detection sensitivity according to $\sqrt{N_o}$. A similar scaling ($\sim \sqrt{N_r}$) holds for a variation in the number of reference stars. As a matter of fact, more reference stars means more unknowns (5 additional astrometric parameters per reference object), but also more differential delay measurements per Standard Visit (as many as the number of reference stars), so that for example doubling N_r or N_o in practice produces similar effects in terms of detectability thresholds. The same scaling applies to the computed errors in measured physical and dynamical quantities of the system, i.e planet mass and orbital elements.

5.3.2. Timing of observations

The choice of the distribution of observations is crucial in many respects: *a*) in terms of the potential for discovery of new planets, it would be desirable to achieve the best sensitivity over a wide range of periods, from a few days to the 5-yr SIM-mission duration; *b*) observation spacing should also be chosen in order to minimize the residual covariance between the orbital

solution for long-period planets and the solution for the parallax and the proper motion of the primary; finally, *c*) in the case of observations of the known candidate planetary systems with one or more planets, it might be necessary to time some observations on the basis of the specific orbital phases, particularly in order to sample adequately the pericenter passage of planets with highly eccentric orbits. The primary focus of the next Section of this paper is to discuss the SIM discovery space in terms of the smallest mass the instrument might be capable to detect around the nearest stars. To this aim, in this Section we attempt to identify the optimum timing of observations required in order to guarantee the performance discussed in point *a*). We pursue this objective by analyzing a sample of possible options for the spacing of SIM observations during the 5-yr mission lifetime, and neglecting for the moment further investigations on the time interval between pairs of quasi-orthogonal observations, randomly chosen in a range of a few days. The optimal time separation will most likely depend on SIM noise model, as well as overheads and other constraints (occultations, exclusion angles), but such issues are not addressed in this paper.

Setting $\sigma_d = 2 \mu\text{as}$, we ran simulations with 200 uniformly distributed star-planet systems chosen to produce scaled signals in the range $1 \leq S \leq 10$, for different choices of the orbital period T , which was allowed to vary in the range 5 days — 5 years, and averaging over other orbital parameters. We used three reference stars per target and distributed $N_o = 24$ full observations over 5 years using a number of different spacings: a) constant with 0.2-yr intervals; b) random uniform; c) proportional to the square of the number of observations ($(3.15/365.25) \times n_{\text{obs}}^2$, where $n_{\text{obs}} = 1, \dots, N_o$); d) geometric series ($1.365^{n_{\text{obs}}}/365.25$); e) logarithmic distribution ($\text{Exp}(\log 2 + \log 900 \times (n_{\text{obs}}/N_o))/365.25$). We performed basic detection analysis via a standard χ^2 test, with confidence level set as usual at 95%, and estimated rms errors on the orbital parameters, for each of the cases mentioned above. The above choices for the time spacing of the observations are only illustrative, and by no means intended to be fully exhaustive, but can be regarded as a useful reference point when considering more sophisticated approaches to this important issue.

The probability of detection is more or less sensitive to the different timing of observations, depending on the value of the orbital period. For T in the range between a few days and ~ 1.5 yr, all distributions are essentially equivalent, and systems with $S \geq 2.2$ are detected with high confidence (95%), regardless of the choice of either of the above spacings. For $1.5 \leq T \leq 5$ yr, the logarithmic and geometric series distributions are less favorable: for example, for $T = 2$ yr and $T = 5$ yr, a scaled signal $S \simeq 3$ and $S \simeq 4$ is required, respectively, in order to reach the 95% detection probability threshold. In fact, with these two choices of time spacing $\sim 80 - 90\%$ of the observations occur within the first 1.5 years, and longer periods suffer from increasingly worse sampling. If $S \leq 2.2$, then different options for the timing of observations do not improve detectability, regardless of the planet’s orbital period. Finally we note that, in the case of equal spacing, aliasing effects are found for periods that happen to be shorter as well as exact integer fractions of the given sampling interval. In such cases, detection probability drops to zero, even for $S \geq 2.2$, as sampling the orbit always at the same point translates in a small additive constant term in the observation equations that is completely absorbed in the least squares solution for the

proper motion.

The situation is somewhat different when we focus on the accuracy in orbit and mass determination. In particular, observations distributed according to the logarithmic sequence or the geometric series are preferable for measuring the orbital elements of planets in a few-days orbits, with an accuracy improvement of roughly 10-20% with respect to the other distributions. In fact, for these two time spacings $\sim 40 - 50\%$ of the observations fall within the first 1-2 months of observing. For an intermediate period range between about 1 month and 1.5 yr, the accuracy in orbit reconstruction is comparable for all the different sampling distributions adopted. When T approaches 5 years, again because of the lack of proper sampling at longer periods, the logarithmic and geometric distributions are less effective with respect to the other timing sequences, and orbital elements suffer a typical loss in accuracy of $\sim 10 - 20\%$. Within the limits of our observational scenario, the above behavior is essentially independent on the value of S . Finally, in the case of constant spacing, as we had already seen in Section 5.2, orbits with periods shorter than the sampling time interval cannot be reconstructed, even when the signal can be easily detected in the observation residuals to the single-star fit.

Orbital eccentricity and inclination are expected to have a non-negligible impact on both detectability and measurability of planets. For example, a significant degradation in accuracy can be expected for eccentric orbits with periods longer than the mission lifetime (see for example Lattanzi et al. (2000a)), due to the fact that deviations from linear motion for a given target may go unrecognized if its orbit around the system barycenter is not sampled in correspondence of the pericenter passage. In the above analysis we find that the values of e and i are not critical in this scenario, as at least one entire orbit is sampled during the 5 years of simulated observations.

For the purpose of this work, we have not analyzed the performance of different orbital spacings for $T \geq 5$ yr, but rather focused on the range of periods over which SIM observations are likely to provide best results. Within the limited scope of this analysis, the relevant results are that distributing the observations according to a logarithmic or geometric series enhances accurate measurements of orbital parameters and masses for orbits of order of a few days, but degrades the probability of detection and orbital elements and mass determination as T approaches the mission lifetime. Instead, a random, uniform distribution or a sequence proportional to the square of the number of observations, less likely to be subject to aliasing effects as in the case of equal sampling intervals, would be the preferred choice in order to achieve the best detection sensitivity and provide more accurate estimates of orbital parameters and masses over orbital periods ranging from ~ 1 month to the mission duration.

5.3.3. *Structure of the Standard Visit for faint targets*

The observing sequence outlined in Section 3.2 and utilized as a template to derive the results reported in Sections 5.1 and 5.2 was only appropriate to bright targets and reference

objects ($V \leq 11$). If the target is fainter than $V = 11$, the structure of the Standard Visit should be modified. Within the constraint given by the 1-hr performance specification period, many possibilities can be investigated, with the primary aim of minimizing the error σ_d on differential delay measurements. We consider two different options which meet the 1-hr constraint. The first consists of extending the integration time on the target during each elemental fringe measurement, up to a maximum of 3.5 minutes, which ensures the time for a target/reference star elemental fringe measurement pair does not exceed 5 minutes including overheads. A possible scenario for a $V = 16$ target consists of observing blocks lasting $5 \times n$ minutes composed of $2 \times 30 \times n$ sec from overheads, $3.5 \times n$ minutes of integration on the target and $30 \times n$ sec of integration on reference stars, which we still assume bright ($V \leq 11$). In this case, the Standard Visit accuracy per relative delay is $\sigma_d = 10.4/\sqrt{N_b}$ μas , driven by the photon error on the target of 10 μas in each 3.5-minute elemental fringe measurement (see Equation 5). In order not to exceed the 1-hr performance specification period, then for $n = 3$ or $n = 6$ reference stars we must require a maximum of $N_b = 4$, or $N_b = 2$, respectively (and consequently $\sigma_d = 5.2$ μas or $\sigma_d = 7.35$ μas). On the other hand, one can conceivably think of increasing the number of observing blocks, keeping the duration of each observing block within $2 \times n$ minutes, as discussed in Section 3.2. A 30-sec integration on both the (faint) target and the (bright) reference objects translates then in a Standard Visit accuracy $\sigma_d = 26.3/\sqrt{N_b}$ μas , and for $n = 3$ and $n = 6$ the limits on the maximum number of observing blocks are $N_b = 10$ and $N_b = 3$, respectively (and consequently $\sigma_d = 8.28$ μas or $\sigma_d = 15.1$ μas). The first scenario is the more efficient, as it allows for the presence of a possibly large number of reference stars (to be preferred for the reasons explained in Section 5.3.1), yet maintaining a higher Standard Visit accuracy even with respect to the best-case scenario for the second observing sequence.

For the purpose of the analysis carried out in the next Section, we use two template observing strategies that take advantage of the observing scenarios discussed and results presented in Sections 3.2, 5.3.1, 5.3.2, and above. In particular, we include 6 bright (all $V \leq 11$), astrometrically clean reference objects per target, and distribute 24 epochs of 2 orthogonal Standard Visits randomly, uniformly spaced in time over the 5-yr SIM mission lifetime. Finally, we adopt somewhat conservative scenarios for the single-measurement error σ_d : *a*) if the target is bright ($V \leq 11$), then each Standard Visit is composed of two unit observing blocks in which are executed 30-sec elemental fringe measurements for target and reference stars, translating on a Standard Visit accuracy $\sigma_d \simeq 3$ μas per each relative delay measurement; *b*) for faint targets, say $V = 16$, the Standard Visit is composed of a single observing block in which are executed 3.5-minute and 30-sec elemental fringe measurements for target and reference stars, respectively, and consequently the single-measurement error on each relative delay is $\sigma_d = 10.4$ μas . In both cases, a Standard Visit lasts approximately half an hour.

5.4. SIM Discovery Space

In Section 5.2 we have shown how SIM’s high-precision astrometric measurements will provide information of great value for the classification of planetary systems and overall assessment of competing theories of planet formation and evolution. In particular, in Section 5.2.2 we have illustrated how extra-solar planets discovered by spectroscopic surveys would fall within SIM’s boundaries for accurate planet detection and measurement, and discussed how they would undoubtedly constitute an important laboratory for SIM. In fact, to go beyond a simple catalogue of extra-solar planets, classification will have to be made on the basis of the knowledge of their true masses, shape and alignment of the orbits, structure and composition of the atmospheres. The dependence of planetary frequencies with age and metallicity will have to be understood. Finally, important issues on planetary systems evolution, such as coplanarity and long-term stability, will have to be addressed. However, the big picture will not be complete without crucial new discoveries. The existence of giant planets orbiting on Jupiter-*like* orbits (4-5 AU, or more), will have to be established. Such objects, when found in systems harboring no close-in giant planets, are the signposts for the discovery of rocky planets in orbits closer to their parent stars, maybe even inside the star’s Habitable Zone, where water is liquid.

We currently have no information about the existence of rocky planets orbiting any other stars, except the rare pulsars (Wolszczan & Frail 1992). SIM’s exquisite astrometric precision will provide the opportunity for detection of planets with a range of masses down to the mass of the Earth around the nearest stars. Answering the age-old question of the uniqueness of our planet as a habitat for life is clearly one of the highest priority objectives of extra-solar planetary science, and the SIM measurements will uniquely complement the expectations coming from other ongoing and planned planet-search surveys, for ground-breaking science in the field of formation and evolution of planetary systems.

We have characterized the limiting performance of SIM in terms of its ability to detect (at the 95% confidence level) Earth-class planets around a given star, as a function of the number of observations. As for the case of physical studies of planetary systems discussed in Section 5.2.2, also here there exists a natural sample of potential targets for observations from which SIM can extract important results: this includes the nearest stars, around which SIM could find planets as small as Earth, if they are present. The nearest stars are significant because their planets are easier to detect by SIM and observe later by new telescopes that can isolate and study their light. Such discoveries would provide prime targets for the Terrestrial Planet Finder (TPF) to characterize spectroscopically in terms of the potential for life.

Our nearest stellar neighbors fall into two main categories for the purpose of SIM observations. The first category consists of the few relatively luminous stars of spectral types K and earlier ($M_{\star} > 0.6 M_{\odot}$). The second category holds the many low-mass, low-luminosity M dwarfs ($M_{\star} < 0.6 M_{\odot}$). The latter are more astrometrically responsive to planets of a given mass; the former includes stars more like the Sun and offers the best opportunity to find habitable planets.

As we have seen in Section 5.1, we can express the mission detection sensitivity in terms of the minimum astrometric signature for discovery α_{\min} , defined by the 95% confidence of detection. This quantity depends on the Standard Visit accuracy σ_d , and within our simplified but realistic observational scenario it scales with the square root of the number of measurement epochs N_o , and of the number of reference stars N_r (see Section 5.3.1). For periods shorter than the mission duration, we found $\alpha_{\min} = 2.2 \sigma_d$.

For any particular star, the boundary of discovery space—the dividing line between detectable and non-detectable—is found by equating α_{\min} to the astrometric signature of the planet, defined by Equation 9. For a given stellar mass and distance of the system, it is then possible to determine the minimum detectable mass $M_{p,\min}$ as a function of the semi-major axis of the planetary orbit a_p . To take into account the loss in sensitivity for periods longer than the mission length L (set to 5 yr), we have parameterized $M_{p,\min}$ as follows:

$$M_{p,\min} = \begin{cases} 2.2 \frac{M_\star D}{a_p} \times \sigma_d \times \sqrt{\frac{24}{N_o}} \times \sqrt{\frac{3}{N_r}} & \text{for } T \leq \frac{7}{9}L \\ 2.2 \frac{M_\star D}{a_p} \times \sigma_d \times \sqrt{\frac{24}{N_o}} \times \sqrt{\frac{3}{N_r}} \times \sin^{-2}\left(\frac{\pi L}{2T}\right) & \text{for } T > \frac{7}{9}L \end{cases}$$

In the plane defined by the mass of the planet M_p and the orbital semi-major axis a_p , this parametric equation identifies a family of curves with the same shape, having an absolute minimum at the value of a_p corresponding to a period $T \simeq 4$ years, where the sensitivity is greatest. The location of the minimum in semi-major axis increases linearly with the distance and with the cube root of the stellar mass, following Kepler’s third law.

To illustrate the potential of SIM for detection of low-mass planets in the vicinity of the solar system, we have selected a sample of 50 nearby stars within 10 pc from the Sun, divided into two sub-samples of 25 stars each belonging to either of the two categories discussed above. As general selection criteria, we have chosen to avoid evolved systems and close binaries (with separations < 10 AU).

For the more massive stars ($M_\star > 0.6 M_\odot$), the main goal is to detect Earth-class planets in the Habitable Zone (HZ). According to the conventional wisdom, a habitable Earth must orbit at a distance from its star where liquid water is stable on its surface. In its classic definition, the inner boundary of the HZ (Kasting et al. 1993) is located at the distance from the star at which a runaway greenhouse effect is generated, which induces water loss via photolysis and hydrogen loss; the outer boundary is located at the distance from the star at which CO_2 clouds start increasing the planet albedo in a way to cool the surface down to the point of freezing water. For low-mass stars this region is very narrow and located at distances much less than 1 AU, while it is wider and located at distances much greater than 1 AU for high-mass stars. The boundaries of this region change in time due to the evolution of the central star, and the concept of Continuously Habitable Zone (CHZ) must be introduced, to identify the region of space around a given star which can be considered habitable at different times. Furthermore, in recent works (Forget & Pierrehumbert 1997; Kasting 1998; Forget 2000) it has been argued that either

CO_2 clouds or the presence of abiotic and/or biogenic CH_4 in the atmosphere should tend to warm a planet’s surface, thus HZs might be significantly wider than previously thought. For the purpose of this investigation, we define operationally the center of the HZ in terms of the orbital period T_{HZ} (in years) and stellar mass M_\star (in solar masses):

$$\frac{T_{HZ}}{T_\oplus} = \left(\frac{M_\star}{M_\odot} \right)^{7/4} \quad (12)$$

This formula, in which T_\oplus is the Earth’s orbital period, roughly holds for Main Sequence stars of spectral type F through K. The inner edge of the HZ is located at $T_{HZ,i} \simeq 0.7 T_{HZ}$, and the outer edge at $T_{HZ,o} \simeq 2 T_{HZ}$.

If a star is not of spectral type K through F, then the characteristics of the HZ change dramatically: very bright and hot stars (spectral type A through O) last far too short a period of time on the Main Sequence (up to a few millions years) to allow for the development of complex life forms (according to the typical time-scales of biological evolution on Earth); M dwarfs instead are thought to be non-ideal environments for harboring a complex biology for two different reasons: *a*) the HZ of a low-mass star is well within the tidal locking radius (Kasting et al. 1993). Whenever synchronous rotation of the star and planet is established, life may be hampered by condensation of the atmosphere on the perpetually cold dark side of the planet; *b*) large stellar flares are common in M-type dwarfs, and they would tend to sterilize life on a regular basis.

Nevertheless, if arguments can be raised against the intrinsic relevance of the HZs of M dwarfs as potential life-sustaining environments, stars of late spectral type are specially interesting because of the more favorable planet/star mass ratio, which allows easier detection of low-mass planets. Furthermore, due to the present results from planet searches being biased towards solar-type stars, issues such as the dependence of planetary frequencies with the spectral type still need to be addressed.

For each of the two stellar sub-samples discussed above, we have set a mass-sensitivity threshold, and determined, within the framework of the two template observing strategies outlined in Section 5.3.3, the number of observations needed to reach it. In particular: 1) for the sub-sample with $M_\star > 0.6 M_\odot$, we have set the mass-threshold for detection to $3 M_\oplus$ at the center of the HZ, except for the case of α Cen A-B, for which, given their proximity to the Sun, we set the goal to be a $1 M_\oplus$ sensitivity at the center of the HZ; 2) for the sub-sample of stars with $M_\star < 0.6 M_\odot$, we have set the same threshold to $1 M_\oplus$ at the most sensitive point of the discovery-space curve, wherever it occurs for each star in semi-major axis (which always corresponds to about a 4-year period).

In Figure 9 we have plotted the parametric equation defining the minimum detectable mass by SIM as a function of semi-major axis for the 10 solar-type stars and for the 14 M dwarfs that require the lowest amount of observations in order to reach the respective goals. The curves relative to each star are color-coded by the number of observations needed to achieve the requested sensitivity. As it can be easily seen, for all the stars in the solar-type sub-sample additional

observations are needed, up to about 6 times the default $N_o = 24$, in the case of η Cas. Instead, we find that 24 observations are sufficient to *exceed* the goal for all of the M dwarfs plotted in Figure 9. As expected, the highest sensitivity is reached in the case of Proxima Cen, where the template observing strategy for a faint target outlined in Section 5.3.3 allows for a minimum detectable mass of $\sim 0.2 M_\oplus$.

These results have been obtained in the context of a somewhat conservative choice for the Standard Visit accuracy for both bright ($V \leq 11$) and faint targets (see Section 5.3.3), and assuming bright reference stars. As a consequence, the amount of full two-dimensional observations needed to achieve the goals of detection of Earth-mass planets in the HZ of solar-type stars within 10 pc from our Sun is very large. Instead, very low-mass planets might be revealed orbiting nearby M dwarfs with more relaxed requests in terms of SIM observing time and single-measurement accuracy.

Our findings are illustrative of some of the many important issues future observing programs with SIM operated in narrow-angle mode will need to debate, at the moment of the final selection of targets. In particular: (a) an optimal tradeoff between the number of stars surveyed and the depth of the search will have to be established; (b) the details of the adopted strategies for observing will have to be refined to maximize the ratio of the number and intrinsic scientific interest of the objects in a target list to the fraction of the total observing time utilized; (c) the specific merit of any particular star itself will have to be discussed, which has both scientific facets (type of star, theories of planet formation) and technical aspects (availability of a robust, bright reference frame, properties of astrometric noise of the target).

6. Summary and Conclusions

Since the establishment of the existence of the first extra-solar planet orbiting a solar-type star (Mayor & Queloz 1995), the approach to sciences of stars and planets has dramatically changed. Now, answers are sought to more advanced questions about the formation and evolution of planetary systems and the existence of rocky, perhaps habitable planets.

Precision astrometry constitutes a fundamental complement to other search techniques. Today, monolithic telescopes and optical interferometers are being built or designed, which will provide accurate astrometric measurements, both from ground (Mariotti et al. 1998; Booth et al. 1999; Colavita et al. 1999) and in space (Danner & Unwin 1999; Röser 1999; Perryman et al. 2001).

In this paper we have used extensive end-to-end numerical simulations of narrow-angle astrometric measurements with the Space Interferometry Mission and the subsequent statistical analysis of the simulated dataset in order to quantify the potential of SIM for the discovery and characterization of single planets around single stars in the vicinity of the solar system. Utilizing a simplified, but realistic, error model for SIM operated in narrow-angle mode, and adopting a reasonable, flexible template observing scenario (Sections 3.2), we have: *a*) defined the bound-

aries for secure planet detection and accurate determination of orbital elements and masses, as function of the basic SIM capabilities and properties of the observed systems (Sections 5.1, 5.2.1, and 5.2.2), *b*) evaluated the impact of different observing strategies on the boundaries for detection and orbit reconstruction (Sections 5.3.1 and 5.3.2); *c*) adopting template observing strategies for both bright ($V \leq 11$) and faint targets (Section 5.3.3), illustrated SIM discovery potential in terms of its ability to detect terrestrial planets around a sample of the closest stars (Section 5.4). Our main results can be summarized as follows.

- (1) secure detection (at the 95% confidence level) will be possible for planets producing an astrometric signature $\alpha_{\min} \sim 2.2$ times larger than the Standard Visit accuracy σ_d , for periods shorter than 5 years, the nominal mission lifetime;
- (2) in the same period range, the mass of the planet and the full set of orbital elements will be determined with a typical accuracy of 20-30% for objects producing a signal $\sim 2\alpha_{\min}$; for mass and inclination measurements accurate to 10%, the required signal is $\sim 10\alpha_{\min}$ and $\sim 15\alpha_{\min}$, respectively; analyzing how the set of presently known extra-solar planets would fall within the boundaries for reliable detection and accurate mass and orbit determination, we find that about 75% will be detected and 50% will have orbital elements and masses measured to 10%, or better;
- (3) the detection threshold scales similarly with the number of observations ($\sqrt{N_o}$) and reference stars ($\sqrt{N_r}$); random uniform and geometric distributions of the observations are preferred for achieving the best detection sensitivity and more accurate estimates of orbital parameters and masses in the period range between ~ 1 month and 5 yr, and ≤ 1 month, respectively;
- (4) due to the very small astrometric signature induced on the parent star, reliable detection of Earth-class planets in the Habitable Zone of the closest solar-type stars will be possible, but demanding in terms of number of full observations per target and measurement precision; instead, around the nearest M dwarfs, more relaxed constraints on the number of observations and single-measurement errors would still ensure detection of planets as small as Earth.

Our findings indicate how SIM, with its unprecedented astrometric precision, will be a valuable tool for discovering planets around stars other than the Sun. Among the new generation of instruments designed to study extra-solar planets, SIM will be able to provide unique insights towards the understanding of planetary systems in their generality and investigating the habitability of other worlds than Earth. Today two factors hamper the transition from the present cataloguing phase to the more fundamental classification phase, where, for example, mass might be operationally used as one of the genesis indicators which would help discriminate between planets and brown dwarfs: *a*) mass uncertainty for the radial-velocity discoveries (due to inclination angle ambiguity), and *b*) incompleteness in the mass range corresponding to solar system planets

(due to inadequate sensitivity). By determining the true rather than the projected orbit of the planet (as with radial-velocity techniques), SIM measurements will remove the inclination angle degeneracy and associated companion-mass uncertainty for the presently existing planets, as well as for those the instrument will discover directly. Furthermore, by ruling out the presence of Earth-mass planets around the nearest stars, SIM will be capable of addressing for the first time the role of rocky cores in the complex scenarios of planetary formation and evolution, and start to investigate their potential habitability. In fact, SIM astrometry will be important in investigating the Habitable Zones of stars with known planets in wide orbits: those systems in which the Habitable Zone and the zone in which planet formation has not been disrupted by the presence of the known giant planet overlap (Wetherill 1996) would immediately become high-priority targets for SIM narrow-angle observations, to search for terrestrial planets and find evidence of the existence of planetary systems resembling our own.

Another crucial area in which SIM measurements might have a significant impact is the study of multiple-planet systems: the remarkable pattern of low-eccentricity orbits and coplanar structure of the solar system are commonly thought to be fossil evidence of the planets having accumulated in a dissipative protoplanetary disk (Lissauer 1993; Pollack et al. 1996). The wide variety of planetary masses and orbits found by radial velocity techniques have called into question the generality of such ideas, suggesting that significant orbital evolution may be needed to explain the high-eccentricity orbits (Artymowicz 1992; Weidenschilling & Marzari 1996; Lin & Ida 1997; Mazeh et al. 1997) and the *Hot Jupiters* at very small orbital radii (Lin et al. 1996; Murray et al. 1998; Lin et al. 2000). By answering the seemingly simple question of whether multiple-planet orbits are coplanar, SIM might confirm that some other planetary systems are similar to our own and similarly indicative of origin in a quiescent, flattened disk. Or, SIM measurements might provide evidence that other systems are truly different, with large relative orbital inclinations, which could point to either an early, chaotic phase of orbital evolution or formation by another mechanism such as disk instability (Kuiper 1951; Cameron 1978; Boss 1997; Boss 2000; Boss et al. 2002). The simulation of SIM observations of extra-solar multiple-planet systems, the quantification of the instrument capability in discovering and measuring systems of planets, as well as its ability in determining coplanarity of multiple-planet orbits, will constitute the core of the results presented in paper II.

Special thanks are due to G. Fritz Benedict, Alan Boss, George Gatewood, Todd Henry, David Latham, and Robert Reasenberg for lending initial impetus and support to this investigation. Over the course of this work, we have benefited from discussions with numerous colleagues, and especially Mike Shao, Steve Unwin, and Dave van Buren. We are also grateful to an anonymous referee for her/his helpful comments. This work has been carried out with the partial financial support of JPL under Contract 960506 to the Space Telescope Science Institute. A.S. and M.G.L. gratefully acknowledge support from the Italian Space Agency under Contract ASI-I/R/117/01.

REFERENCES

- Artymowicz, P. 1992, *PASP*, 104, 769
- Barnes, R., Quinn, T. 2000, *ApJ*, 550, 884
- Basri, G. & Marcy, G. W. 1997, in *AIP Conf. Proc. 393, Star Formation, Near and Far*, ed. S. Holt & L. G. Mundy (New York, AIP), 228
- Black, D. 1997, *ApJ*, 490, L171
- Bodenheimer, P., Hubickyj, O., Lissauer J. J. 2000, *Icarus*, 143, 2
- Booth, A. J., et al. 1999, in *Working on the Fringe: Optical and IR Interferometry from Ground and Space*, ed. S. Unwin & R. Stachnik, *ASP Conf. Series 194*, 256
- Boss, A. P. 1997, *Science*, 276, 1836
- Boss, A. P. 2000, *ApJ*, 536, L101
- Boss, A. P. 2002, *ApJ*, 567, L149
- Boss, A. P., Wetherill, G. W., Haghighipour, N. 2002, *Icarus*, 156, 291
- Butler, R. P., Marcy, G. W., Williams, E., McCarthy, C., Vogt, S. S. 1996, *PASP*, 108, 500
- Butler, R. P., Marcy, G. W., Williams, E., Hauser, H., Shirts, P. 1997, *ApJ*, 474, L115
- Butler, R. P., Marcy, G. W., Fischer, D. A., Brown, T. M., Contos, A. R., Korzennik, S. G., Nisenson, P., Noyes, R. W. 1999, *ApJ*, 526, 916
- Butler, R. P., Marcy, G. W., Fischer, D. A., Vogt, S. S., Tinney, C. G., Jones, H. R. A., Penny, A. J., Apps, K. 2000, in *Planetary Systems in the Universe: Observation, Formation and Evolution*, *IAU Symp. 202*, ed. A. Penny, P. Artymowicz, A. M. Lagrange & S. Russell, in press
- Cameron, A. G. W. 1978, *Moon Planets*, 18, 5
- Campbell, B., Walker, G. A. H., Yang S. 1988, *ApJ*, 331, 902
- Casertano, S., Sozzetti, A. 1999, in *Working on the Fringe: Optical and IR Interferometry from Ground and Space*, ed. S. Unwin & R. Stachnik, *ASP Conf. Series 194*, 171
- Charbonneau, D., Brown, T. M., Latham, D. W., Mayor, M. 2000, *ApJ*, 529, L45
- Charbonneau, D., Brown, T. M., Noyes, R. W., Gilliland, R. L. 2002, *ApJ*, 568, 377
- Cochran, W. D., Hatzes, A. P. Marcy, G. W., Butler, R. P. 1997, *ApJ*, 483, 457

- Colavita, M. M., et al. 1999, *ApJ*, 510, 505
- Danner, R., Unwin, S. 1999, *SIM: Taking the Measure of the Universe*, NASA/JPL
- Del Popolo, A., Ekşi, K. Y. 2002, *MNRAS*, 332, 485
- Els S. G., Sterzik M. F., Marchis F., et al. 2001, *A&A*, 370, L1
- Fischer, D. A., Marcy, G. W., Butler, R. P., Laughlin, G., Vogt, S. S. 2002, *ApJ*, 564, 1028
- Forget, F., Pierrehumbert. R. T. 1997, *Science*, 278, 1273
- Forget, F. 2000, *Earth, Moon, and Planets*, 81, 59
- Gatewood, G., Han, I., Black, D. C. 2001, *ApJ*, 548, L61
- Gilmore, G., et al. 2000, *Proc. SPIE 4013, UV, Optical, and IR Space Telescopes and Instruments*, ed. J. B. Breckinridge & P. Jacobsen, 453
- Gonzalez, G., Laws, C., Tyagi, S., et al. 2001, *AJ*, 121, 432
- Green, R. 1985, *Spherical Astronomy* (Cambridge University Press)
- Gürsel, Y. 1993, *Proc. SPIE 1947, Space-borne Interferometry*, ed. R. D. Reasenberg, 188
- Halbwachs, J. L., Arenou, F., Mayor, M., et al. 2000, *A&A*, 355, 581
- Halbwachs, J. L., Arenou, F., Mayor, M., et al. 2001, in *Birth and Evolution of Binary Stars*, IAU Symp. 200 Poster Book, ed. B. Reipurth & H. Zinnecker, 132
- Han, I., Black, D. C., Gatewood, G. 2001, *ApJ*, 548, L57
- Heacox, W. D. 1999, *ApJ*, 526, 928
- Henry, G. W., Marcy, G. W., Butler, R. P., Vogt, S. S. 2000, *ApJ*, 529, L41
- Jorissen, A., Mayor, M., Udry, S. 2001, *A&A* 379, 992
- Kasting, J. F., Whitmire, D. P., Reynolds, R. T. 1993, *Icarus*, 101, 108
- Kasting, J. F. 1998, *BAAS*, 30, 1328
- Konacki, M., Maciejewski, A. J., Wolszczan, A. 2002, *ApJ*, 567, 566
- Kuhnert, A. C., et al. 1998, *Proc. SPIE 3350, Astronomical Interferometry*, Ed. R. D. Reasenberg, 100
- Kuhnert, A. C., et al. 2000, *Proc. SPIE 4006, Interferometry in Optical Astronomy*, ed. P. J. Lena & A. Quirrenbach, 815

- Kuiper, G. P. 1951, Proc. Natl. Acad. Sci. USA, 37, 1
- Lattanzi, M. G., Spagna, A., Sozzetti, A., Casertano, S. 1997, Proc. ESA Symp., Hipparcos - Venice '97, ESA SP-402, 755
- Lattanzi, M. G., Spagna, A., Sozzetti, A., Casertano, S. 2000a, MNRAS, 317, 211
- Lattanzi M.G., Sozzetti A., Spagna A. 2000b, in From Extra-solar Planets to Cosmology: The VLT Opening Symposium, ed. J. Bergeron & A. Renzini (Berlin: Springer-Verlag), 479
- Laughlin, G., Adams, F. C. 1999, ApJ, 526, 881
- Laughlin, G. 2000, ApJ, 545, 1064
- Leitch, J. W., Kopp, G. A., Noecker, C. 1998, Proc. SPIE 3350, Astronomical Interferometry, Ed. R. D. Reasenberg, p. 526
- Lin, D. N. C., Bodenheimer, P., Richardson, D. 1996, Nature, 380, 606
- Lin, D. N. C., Ida, S. 1997, ApJ, 477, 781
- Lin, D. N. C., Papaloizou, J. C. B., Terquem, C., Bryden, G., Ida, S. 2000, in Protostars and Planets IV, ed V. Mannings, A. P. Boss & S. S. Russell (Tucson: University of Arizona Press), p. 1111
- Lissauer, J. J. 1993, ARA&A, 31, 129
- Marcy, G. W., Benitz, K. J. 1989, ApJ, 344, 441
- Marcy, G. W., Butler, R. P. 1994, in Proc. ESO Workshop, The Bottom of the Main Sequence - and Beyond, ed. C. G. Tinney (Springer-Verlag, Heidelberg), 98
- Marcy, G. W., Butler, R. P. 1998, ARA&A, 36, 57
- Marcy G. W., Butler R. P., Fischer D., et al. 2001a, ApJ, 556, 296
- Marcy G. W., Butler R. P., Vogt S. S., et al. 2001b, ApJ, 555, 418
- Mariotti, J. M., et al. 1998, Proc. SPIE 3350, Astronomical Interferometry, Ed. R. D. Reasenberg, p. 800
- Mayor, M., Queloz, D. 1995, Nature, 378, 355
- Mayor, M., Queloz, D., Udry, S. 1998a, in Brown Dwarfs and Extrasolar Planets, ed. R. Rebolo, E. L. Martin & M. R. Zapatero-Osorio (S. Francisco, ASP), 140
- Mayor, M., Udry, S., Queloz, D. 1998b, in ASP Conf. Ser. 154, Tenth Cambridge Workshop on Cool Stars, Stellar Systems, and the Sun, ed. R. Donahue & J. bookbinder (S. Francisco, ASP), 77

- Mayor, M. & Udry, S. 2000, in *Disks, Planetesimals, and Planets*, ed. F. Garzón, C. Eiroa, D. de Winter & T. J. Mahoney, ASP Conf. Series, 219
- Mazeh, T., Latham, D. W., Stefanik, R. P. 1996, *ApJ*, 466, 415
- Mazeh, T., Krymolowski, Y., Rosenfeld, G. 1997, *ApJ*, 477, L103
- Mazeh, T. & Zucker, S. 2001, in *Birth and Evolution of Binary Stars*, IAU Symp. 200, ed. R. D. Mathieu & H. Zinnecker, 519
- Murray, N., Hansen, B., Holman, M., Tremaine, S. 1998, *Science*, 279, 69
- Neat, G. W., Abramovici, A. R., Calvet, R. J., Korechoff, R. P., Joshi, S. S., Goullioud, R. 1998, *Proc. SPIE 3350, Astronomical Interferometry*, Ed. R. D. Reasenberg, p. 1020
- Noecker, M. C. 1995, *Proc. SPIE 2477, Space-borne Interferometry II*, ed. R. D. Reasenberg, 188
- Oppenheimer, B. R., Kulkarni, S. R., Stauffer, J. R. 2000, in *Protostars and Planets IV*, ed V. Mannings, A. P. Boss & S. S. Russell (Tucson: University of Arizona Press), p. 1313
- Perryman, M. A. C., et al. 2001, *A&A*, 369, 339
- Pollack, J. B., Hubickyj, O., Bodenheimer, P., Lissauer, J. J., Podolack, M., Greenzweig, Y. 1996, *Icarus*, 124, 62
- Pourbaix, D. 2001, *A&A*, 369, L22
- Pourbaix, D., Arenou, F. 2001, *A&A*, 372, 935
- Press, W. H., Teukolsky, S. A., Vetterling, V. T., et al. 1992, *Numerical recipes in FORTRAN: the art of scientific computing*, Cambridge University Press
- Reasenberg, R. D., et al. 1995, *Proc. SPIE 2477, Space-borne Interferometry II*, ed. R. D. Reasenberg, 167
- Reasenberg, R. D., Babcock, R. W., Chandler, J. F., Phillips, J. D. 1997, in *Planets Beyond the Solar System*, ASP Conf. Series 119, ed. D. R. Soderblom, p. 91
- Rivera, E. J., Lissauer, J. J. 2000, *ApJ*, 530, 454
- Röser, S. 1999, in *Working on the Fringe: Optical and IR Interferometry from Ground and Space*, ed. S. Unwin & R. Stachnik, ASP Conf. Series 194, 121
- Santos, N. C., Israelian, G., Mayor, M. 2001, *A&A*, 373, 1019
- Shaklan, S. B., et al. 1998, *Proc. SPIE 3350, Astronomical Interferometry*, Ed. R. D. Reasenberg, 1009
- Sozzetti, A., Spagna, A., Lattanzi, M. G. 2000, *Earth, Moon, and Planets*, 81, 103

- Sozzetti, A., Casertano, S., Lattanzi, M. G., Spagna A. 2001, *A&A*, 373, L21
- Stepinski, T. F., Black, D. C. 2000, *A&A*, 356, 903
- Stepinski, T. F., Black, D. C. 2001, *A&A*, 371, 250
- Stepinski, T. F., Malhotra, R., Black, D. C. 2000, *ApJ* 545, 1044
- Trilling, D., Benz, W., Guillot, T., Lunine, J. I., Hubbard, W. B., and Burrows, A. 1998, *ApJ*, 500, 428
- Udry S., Mayor M., & Queloz D., 2000, in *Planetary Systems in the Universe: Observation, Formation and Evolution*, IAU Symp. 202, ed. A. Penny, P. Artymowicz, A. M. Lagrange & S. Russell, in press
- Ward, W. R. 1997, *ApJ*, 482, L211
- Weidenschilling, S. J., Marzari, F. 1996, *Nature*, 384, 619
- Wetherill, G. W. 1996, *Icarus*, 119, 219
- Wolszczan, A., Frail, D. A. 1992, *Nature*, 355, 145
- Wuchterl, G. 1997, in *Science with the VLT Interferometer*, ed. F. Paresce (Berlin, Springer & Verlag) , p. 64
- Zucker, S. & Mazeh, T. 2001a, *ApJ*, 562, 549
- Zucker, S. & Mazeh, T. 2001b, *ApJ*, 562, 1038

Fig. 1.— Equal probability contours for planet detection at 95% confidence, as a function of orbital period T and astrometric signature α . Detection probability averaged over all other orbital parameters. The dashed lines indicate the equivalent signature at the given distance for a solar-mass primary and for a $20 M_{\oplus}$ planet ($1 M_J$ in parenthesis)

Fig. 2.— Isoprobability contours for various detection probabilities as function of the orbital period T and the distance D , for a $1-M_J$ planet orbiting a $1 M_{\odot}$ star

Fig. 3.— Detection probability as function of the ratio between astrometric signature α and single-measurement error σ_d , for various orbital periods

Fig. 4.— Orbital fits for 200 simulations of a $1-M_J$ planet around a $1-M_{\odot}$ star with a 1-yr (black histograms), 5-yr (red histograms), and 12-yr (yellow histograms) period, at $D = 100$ pc ($\alpha \simeq 10 \mu\text{as}$), 200 pc ($\alpha \simeq 15 \mu\text{as}$), and again 100 pc ($\alpha \simeq 50 \mu\text{as}$), respectively. The panels present the distributions of the fitted values of the most relevant parameters with respect to their “true” values. Eccentricity, inclination, and phases are chosen randomly for each simulated system. The 1-yr periodicity is best determined, while slightly larger errors on the parallax and semi-major axis are evidence for the (weak) coupling between orbital period and parallactic motion

Fig. 5.— The motion on the sky of a system composed of a $1-M_{\odot}$ star and a $1-M_J$ planet on a 5-yr period, at $D = 200$ pc, as ‘seen’ by SIM during its 5-yr mission. In the two upper panels the solid lines represent the true motion along the X- and Y-axis, the triangles are the computed positions at the epochs of SIM observations, after the single-star fit. The post-fit residuals, as function of the time of observations, are shown as diamonds in the relative sub-panels, clearly highlighting the presence of the periodic perturbation due to the orbiting planet; the lower left panel shows the combined apparent motion of the system on the sphere in two dimensions (solid line), and superposed the fitted positions at the epochs of SIM observations (asterisks)

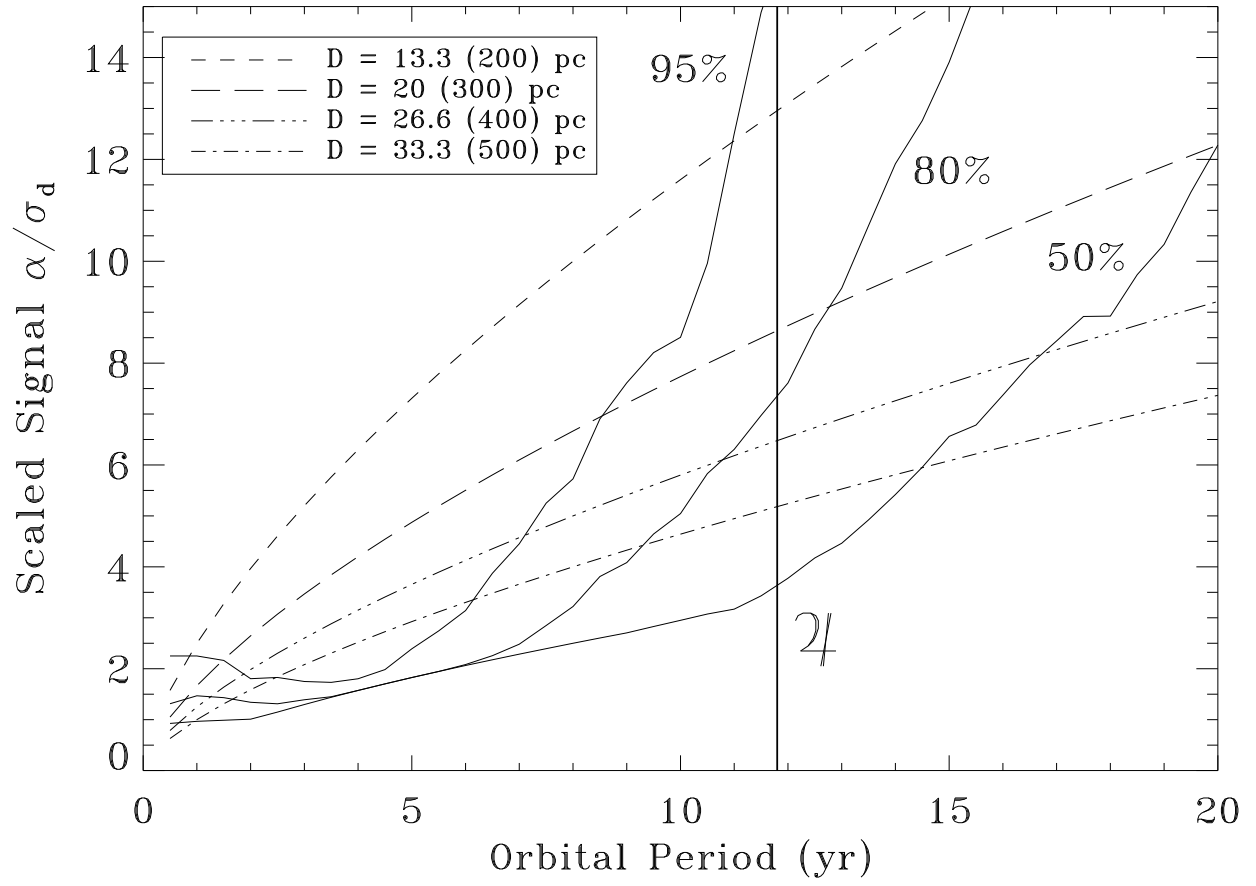
Fig. 6.— The orbital motion of the central star in the system of Figure 5 around the common barycenter: the solid line in the upper two panels represents the true orbit of the star projected on the X- and Y-axis, respectively, while the squares are the computed positions at the epochs of SIM observations, after the full Keplerian fit; in the two sub-panels the post-fit observation residuals as a function of the time of observations reveal do not reveal any additional periodic behavior, and are consistent with the measurement errors, providing confirmation of the high accuracy in the reconstruction of the planetary orbit (as shown by the rms errors on the fitted parameters in Figure 4); the two lower panels show the combined orbital motion of the star in two dimensions (solid line), and superposed the epochs of SIM observations after the single-star fit (crosses in the lower left panels) and after the full orbital fit (asterisks in the lower right panel), respectively

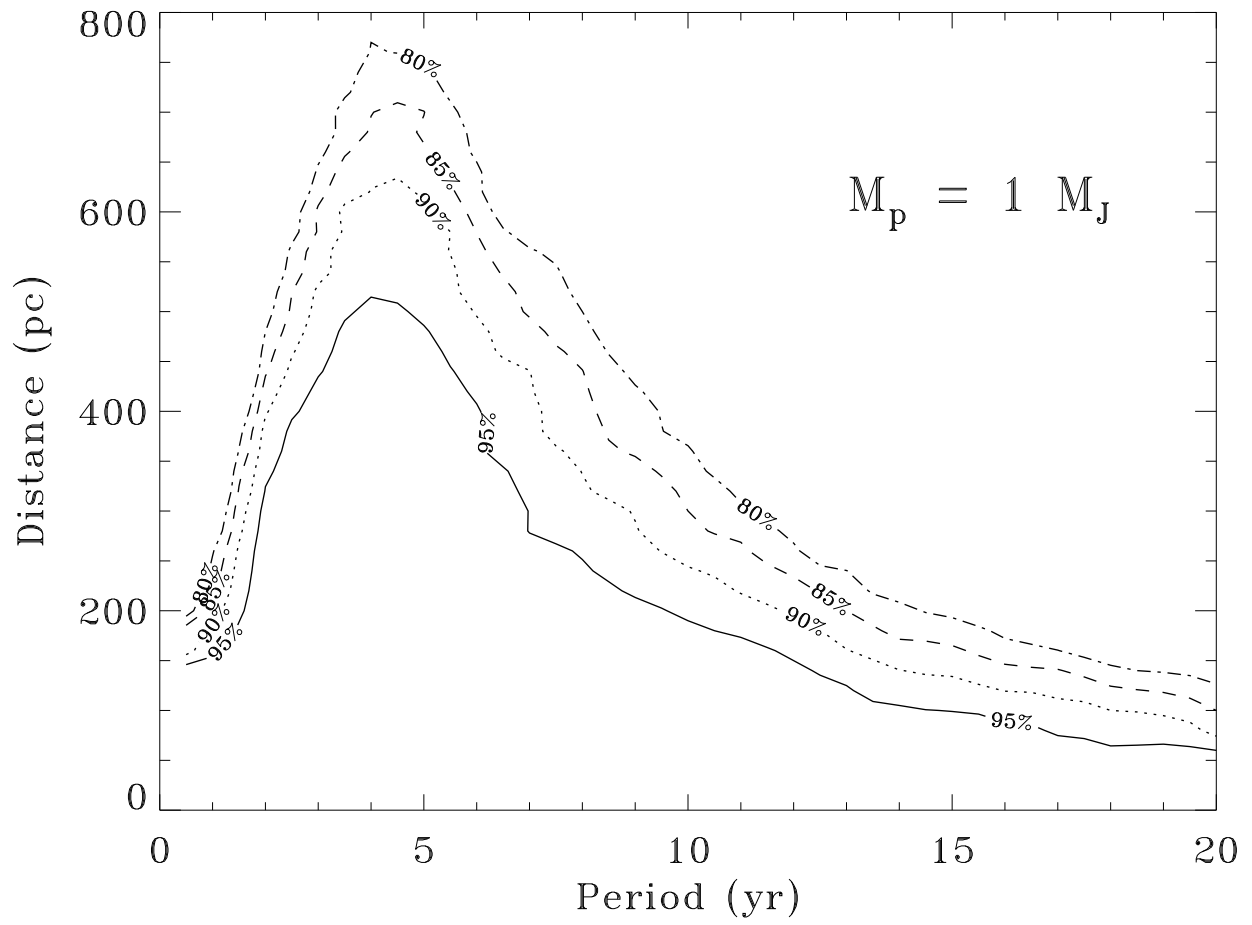
Fig. 7.— The boundaries of secure detection and accurate mass and orbital parameters determination compared to the known extra-solar planets, which are plotted for the *minimum* case: orbit viewed edge-on, true mass equals radial-velocity minimum mass, and astrometric signature minimum. The radius of each planet’s symbol is proportional to the cube root of the minimum mass.

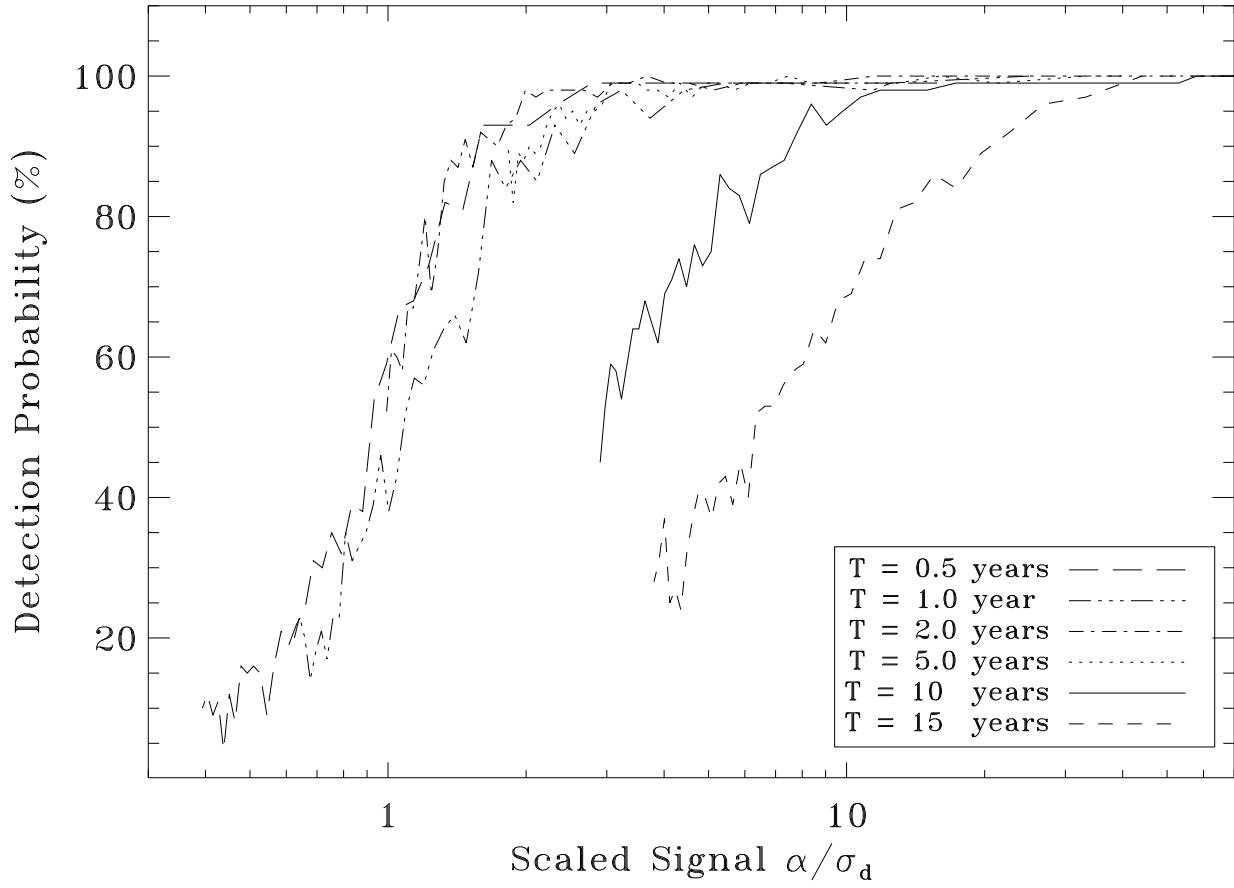
As described in the text, lines of different shape represent the minimum astrometric signature for 95% probability of detection (solid), the minimum astrometric signature for 10% accuracy measurements of the (minimum) mass of the planet (dashed-dotted), and the minimum astrometric signature for 10% accuracy measurements of the (maximum) inclination angle (dashed), respectively. The true astrometric signature, which is proportional to the true mass, will be generally higher—much higher in some cases—with the effect that more reliable detections and orbital fits will be possible

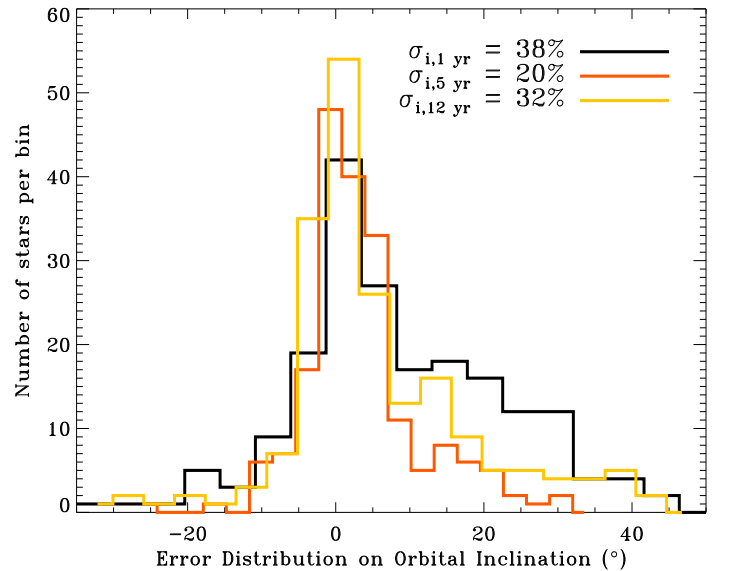
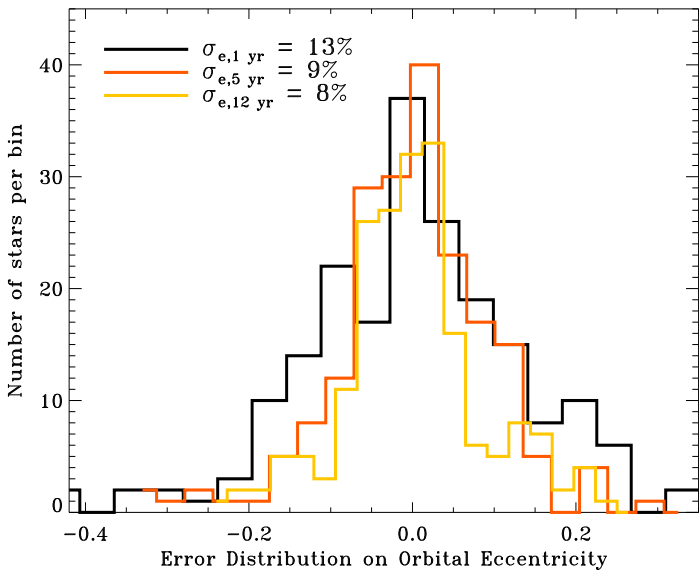
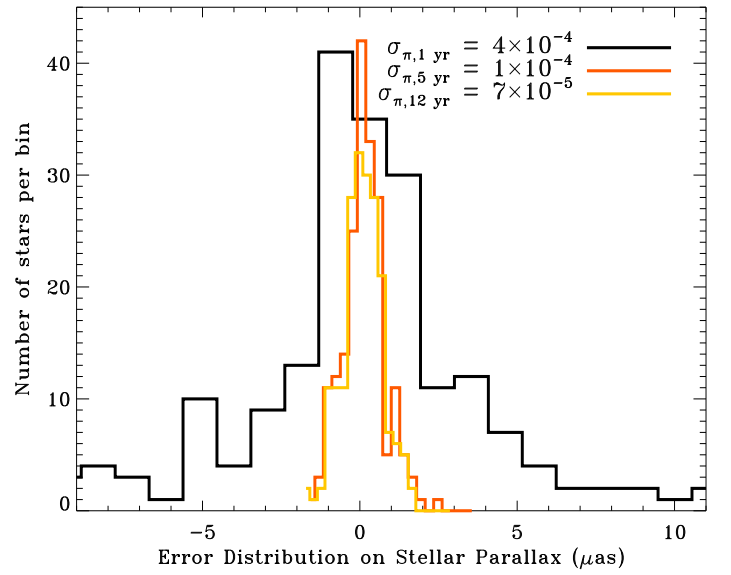
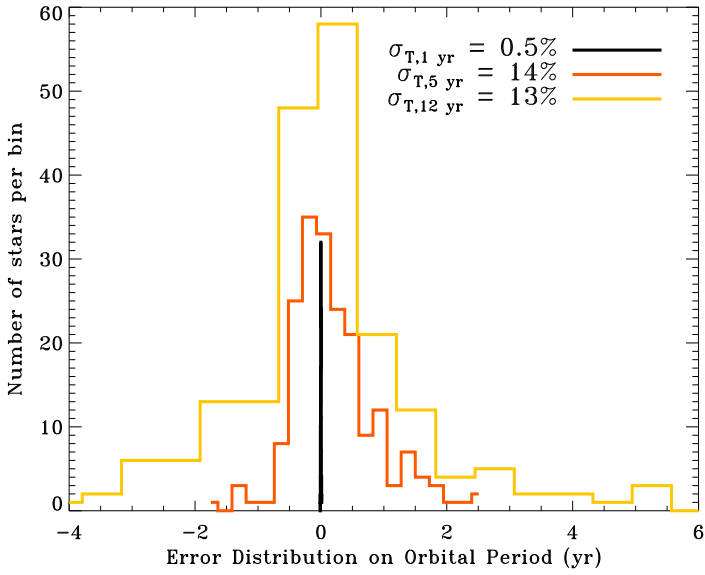
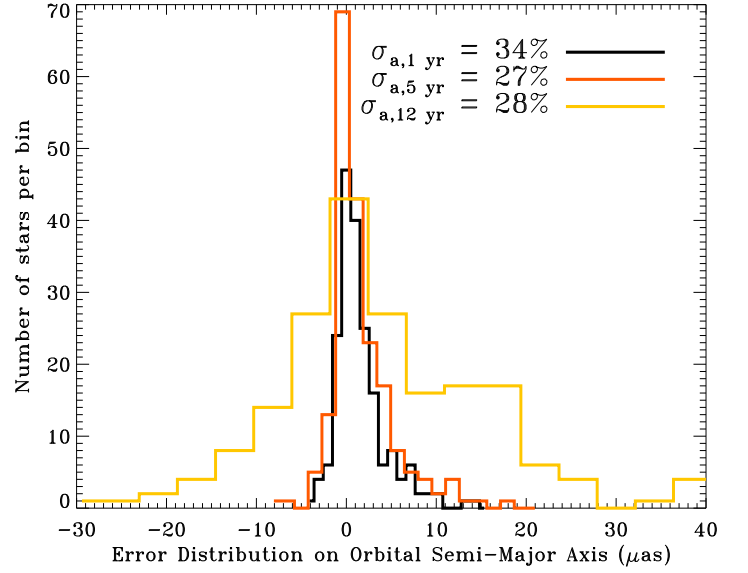
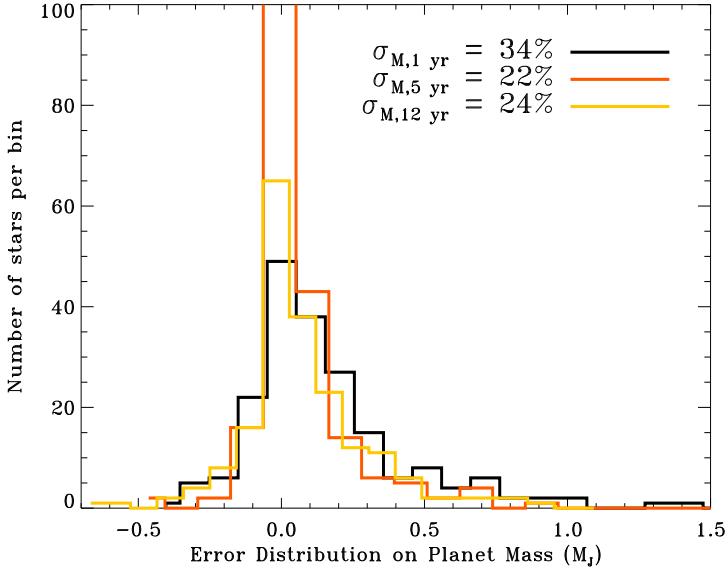
Fig. 8.— Detection horizon vs. number of two-dimensional observations for 3 and 6 reference stars, and for a Jupiter-Sun system with orbital period $T = 5$ years (near the peak in the detectability curves in Figures 1 and 2). A detection probability $P \geq 95\%$ is assumed

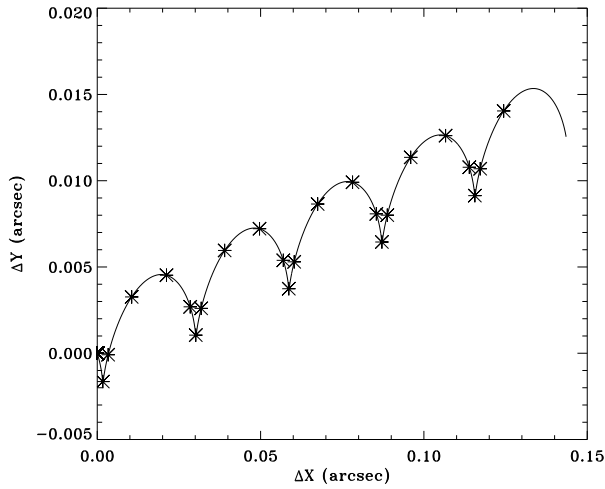
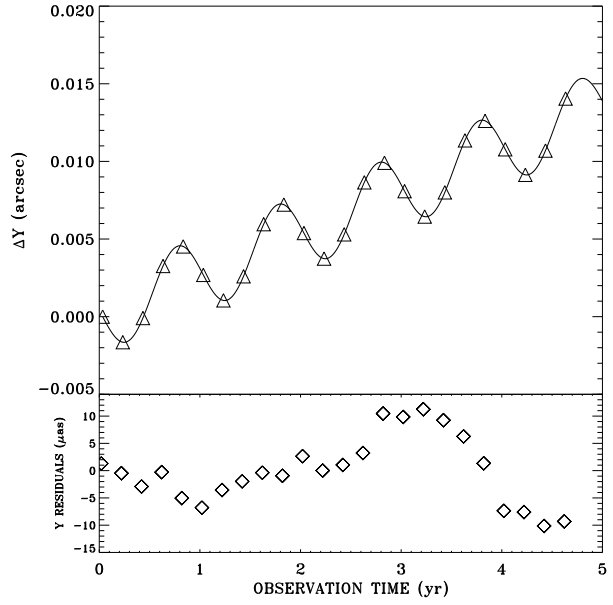
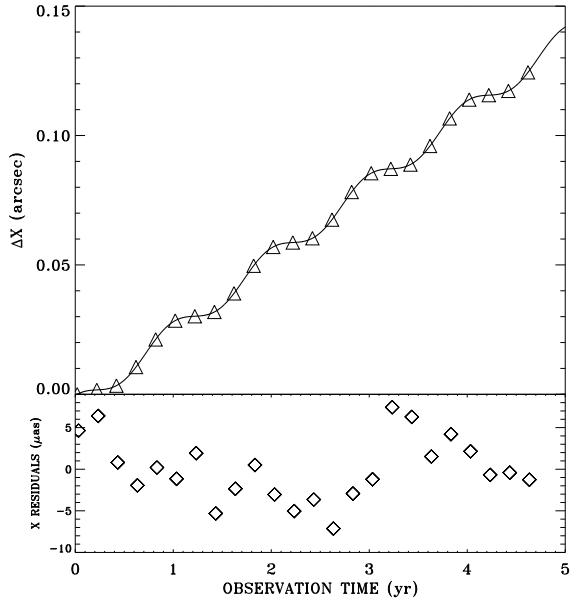
Fig. 9.— Detectable mass as a function of semi-major axis for a sample of stars within 10 pc from the Sun. Discoverable planets lie above the solid curve for each target. Curves are color-coded by number of observations, from yellow (minimum of 24 full observations with the template observing strategies outlined in Section 5.3.3) to green (maximum of 130 observations for η Cassiopeiae); the color scale is shown in the lower-right corner. The minimum of each curve corresponds to a period of 4 years, where the sensitivity is greatest; the steep rise to the right illustrates the loss of sensitivity as the period approaches and exceeds the mission duration. The position of the vertex moves from the left (M dwarfs) to the right as the stellar mass increases; for clarity, only the vertex is shown for several M dwarfs. The curves for Gl 702 A and τ Ceti overlap; both labels are listed for one curve (all curves have the same shape). The thick blue segment shows the approximate Habitable Zone around each star. For low-mass stars, the Habitable Zone falls to the left of the graph. The diagonal purple line corresponds to best-case detectability by radial-velocity searches (edge-on orbit) with an accuracy of 1 m/s, assuming $M_\star = 1M_\odot$











Star = $1 M_{\odot}$
Planet Mass = $1 M_J$
Distance = 200 pc
Orbital Period = 5 years
Eccentricity = 0.60
24 2-d observations
3 reference stars
144 relative delay measurements
 χ^2 (single-star fit) = 857.9
 χ^2 (orbital fit) = 131.2

